SC-CR-66-2128

F6

AEROSPACE NUCLEAR SAFETY

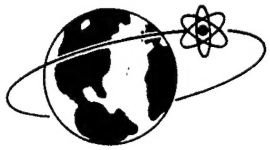

SC-CR-66-2128

November 1966

FEASIBILITY STUDY ON SMALL PARTICLE ABLATION USING A FREE-FLIGHT RANGE (U)

Prepared by
Daniel J. Collins, David K. Sangster, and Walter K. Rogers
GM Defense Research Laboratories
General Motors Corporation
Santa Barbara, California

Reproduced From
Best Available Copy

DISTRIBUTION STATEMENT A
Approved for Public Release
Distribution Unlimited

20011019 120

LOVELACE FOUNDATION
DOCUMENT LIBRARY

SANDIA CORPORATION

PRIME CONTRACTOR TO THE U.S. ATOMIC ENERGY COMMISSION | ALBUQUERQUE, NEW MEXICO; LIVERMORE, CALIFORNIA; TONOPAH, NEVADA

Issued by Sandia Corporation,
a prime contractor to the
United States Atomic Energy Commission

LEGAL NOTICE

This report was prepared as an account of Government sponsored work. Neither the United States, nor the Commission, nor any person acting on behalf of the Commission:

A. Makes any warranty or representation, expressed or implied, with respect to the accuracy, completeness, or usefulness of the information contained in this report, or that the use of any information, apparatus, method, or process disclosed in this report may not infringe privately owned rights; or

B. Assumes any liabilities with respect to the use of, or for damages resulting from the use of any information, apparatus, method, or process disclosed in this report.

As used in the above, "person acting on behalf of the Commission" includes any employee or contractor of the Commission, or employee of such contractor, to the extent that such employee or contractor of the Commission, or employee of such contractor prepares, disseminates, or provides access to, any information pursuant to his employment or contract with the Commission, or his employment with such contractor.

Printed in USA. Price $3.00. Available from the Clearinghouse for Federal Scientific and Technical Information, National Bureau of Standards
U. S. Department of Commerce, Springfield, Virginia 22151

SC-CR-66-2128

FEASIBILITY STUDY ON SMALL PARTICLE ABLATION USING A FREE-FLIGHT RANGE (U)

Prepared by

Daniel J. Collins
David K. Sangster
Walter K. Rogers

GM Defense Research Laboratories, General Motors Corporation
Santa Barbara, California

for

Sandia Corporation

under

Contract 48-4587

ABSTRACT

The feasibility of using a free-flight range to investigate the re-entry behavior of small spherical particles (400 to 700 microns diameter) was experimentally investigated.

Using laser photography, information was obtained of shape changes of particles in flight. Under the conditions of the experiments, it is concluded that Al_2O_3 spheres fragment as a result of thermal stresses.

November 1966

SUMMARY

Safety analysis for space nuclear power supplies frequently requires that the reentry ablation behavior of small spherical particles be predicted. Since ballistic free-flight ranges are the only existing laboratory facility capable of simultaneously simulating all of the reentry variables, a feasibility study, sponsored by Sandia Laboratory, was carried out by the General Motors Defense Research Laboratories.

The objective of this study was to determine the feasibility of launching small spherical particles in the diameter range of 200 to 800 microns at high velocity and obtain useful data on ablation behavior using the latest techniques in laser photography. Spheres of crystalline aluminum oxide (Al_2O_3), supplied by Sandia, were used for the experiments.

The particles actually fired in the experiments varied from 400 to 700 microns in diameter and were launched at velocities from 7 km/sec to 8 km/sec. The range gas was air, and the range pressures varied from 25mm to 50mm of mercury.

Laser photographs and shadowgraphs of the particles in flight showed size and shape changes, and the laser schlieren delineated the flow field about the particles. (A Beckman and Whitley isodensitracer was used in the laser shadowgraph data reduction.) From analysis of the data and considerations of thermal stress levels, it is concluded that mechanical breakup of the particles occurred during flight.

CONTENTS

ILLUSTRATIONS

INTRODUCTION

Safety analysis for space nuclear power supplies frequently requires that the reentry ablation behavior of small spherical particles be predicted. Since ballistic free-flight ranges are the only existing laboratory facility capable of simultaneously simulating all of the reentry variables, a feasibility study, sponsored by Sandia Laboratory, was carried out by the General Motors Defense Research Laboratories.

The objective of this study was to determine the feasibility of launching small spherical particles in the diameter range of 200 to 800 microns at high velocity and obtain useful data on ablation behavior using the latest techniques in laser photography. Spheres of crystalline aluminum oxide (Al_2O_3), supplied by Sandia, were used for the experiments.

The particles actually fired in the experiments varied from 400 to 700 microns in diameter and were launched at velocities from 7 km/sec to 8 km/sec. The range gas was air, and the range pressures varied from 25mm to 50mm of mercury.

Laser photographs and shadowgraphs of the particles in flight showed size and shape changes, and the laser schlieren delineated the flow field about the particles. (A Beckman and Whitley isodensitracer was used in the laser shadowgraph data reduction.)

DESCRIPTION OF FREE-FLIGHT RANGE AND INSTRUMENTATION

Since models can be launched at full reentry velocity into a controlled atmosphere in the free-flight range, the full simulation of flow field about the model is possible.

The top of Figure 1 shows a scaled schematic of the light-gas gun used to launch models at specified velocities. The gun is operated by firing a powder charge which drives a piston into the pump tube, compressing the light gas (typically hydrogen) to a high pressure and temperature. The release of a diaphragm, or break valve, allows the gas to impel a sabot containing the model at a velocity of around 8 km/sec.[1] The bottom half of Figure 1 shows the location of instrumentation used for the microsphere test. A pair of spark shadowgraphs at each end of the range provide data on velocity at the beginning and end of each test. In addition, the instrumentation includes three Q-switched laser stations, as follows:

(1) Laser schlieren station
(2) Laser photograph station (simultaneous shadowgraphs)
(3) TBL laser shadowgraph station

Figures 2, 3 and 4 are schematics of the operation of these three pieces of equipment. (Not shown are the filters which prevent all light but the laser (6943A) from reaching the film, so that strongly ablating models can be photographed without overexposing the film.)

A Calumet view camera (4x5) was adjusted to a depth of field of about 3 inches around the firing line of the range for the laser photographs, made with Type 413 infrared Polaroid film. Simple Polaroid backs with positive-negative film (P/N 55) were used for the shadowgraphs and schlieren; the collimating lenses were Eastman Aero Ektar f:2.5. The P/N 55 negative film is capable of a resolution of approximately 155 lines/mm, although the optics of the system degrade the resolution to around 100 lines/mm.

An open-shutter streak camera provided some streak data on the particles; in addition, target photos gave some information about breakup at impact. (Problems in triggering, sensitivity, and equipment prevented getting any time-differentiated spectrographic data with an STL image converter camera.)

ANALYTICAL STUDIES

In the computer investigations to determine the point in the range where ablation begins, a computer program obtained from Aerospace Corporation was used.[2] The Handbook of Thermophysical Properties[3] provided the material properties for Al_2O_3 (Fig. 5). Figure 6, surface temperature as a function of range distance for different range pressures and sphere diameters, shows that the melting temperature is reached after a flight of 1 to 3 meters. (In this analysis the particle is treated as one-dimensional, and no correction has been made for small particle size, as indicated by Matula.[4]) Figure 7 shows both the fairly steep temperature gradient in the body from a 400μ-diameter particle and the percentage linear thermal expansion.

Although the analysis is not valid after the melting temperature is reached, some idea of the surface change to be expected during flight can be obtained by treating the Al_2O_3 as a subliming ablator. Figure 8 shows the results of this one-dimensional surface analysis. With the present experimental setup, changes of around 10 μ would be expected.

Other calculations for the data runs (Figs. 9 — 14) included velocity and heat input as a function of range distance (using an on-line computer), and the equilibrium temperature of the particle (based on the assumption that heat input during flight raised the temperature of the entire particle).

EXPERIMENTAL RESULTS

Microparticles ranging from 400 μ to 700 μ were fired at velocities up to 8 km/sec. Before these firings, the smallest sphere that had been fired in the Flight Physics Laboratory was 800 μ. Throughout the program, conventional firing techniques and modified range shadowgraphs were employed, with particular care given to alignment, cleanliness, light intensity, and trigger sensitivity.

An improved amplifier and a narrow light fence were used in the shadowgraph triggering network at the beginning of the range; the shadowgraphs at the end of the range were triggered by light emitted from the ablating model. A 1P21 photomultiplier with an emitter-follow-amplifier was used for the triggers at the end, as well as for all other range instrumentation.

In Figure 15, typical trigger signals obtained from a 700-μ particle, the traces for interrupted light triggers show the amplified signal for the first pair of shadowgraph stations, A and B; the traces for the emission trigger from the laser photograph station include the original signal and the amplified signal. Even though the detection of particles will become increasingly difficult as they become smaller and smaller, these tests indicate that the trigger instrumentation developed for this program was adequate.

Figures 16 and 17 show a typical model (700μ) and sabot magnified ten times. Instead of carrying a "cloud" of models, each sabot carried only a single particle during launching.

Table I summarizes all the firings in this program. Even though results were very acceptable ballistically, future programs are expected to be even more successful. Some of the firing failures were caused by the destruction of the model by impact with fragments of the sabot at the separator, a problem not usually met in conventional range operation; that is, models ordinarily outrun pieces of the sabot during separation. In these tests, however, pieces of the sabot outran the model, creating a cloud of debris through which the model had to fly. The sabot separator has since been redesigned.

Most of the data from the tests is photographic. In a typical shadowgraph record at the beginning of the range (Fig. 18), the flow field is clearly evident, as is the distinct smear of the particle, a result of the duration of the spark source. A comparison of this record with the laser data shows the great advantage of the laser's short pulse.

One of the two photographs obtained from the laser schlieren data is shown in Figure 19 (reduced because the schlieren mirror is 12 inches in diameter), and streak pictures which record some indication of particle breakup in two of the data runs are shown in Figure 20.

Figure 21 shows the type of impact information obtained from some of the shots: Run 1209 indicates a clean impact of one particle, despite photographic evidence that the particle had fragmented; run 1186, which did not produce laser pictures, indicates the impact of a larger particle with many small particles near the main crater. From the impact data, the particles seem to range from 8μ to over 100μ at velocities similar to that of the primary particle. Since these smaller particles have a low ballistic coefficient, their velocity decreases faster than the velocity of the primary particle; hence they are assumed to have broken away from the primary particle just before impact. Additional confirmation that the primary particle has indeed decreased in size due to particle breakup in flight comes from the size of the crater formed by the primary particle; that is, the crater was formed by a particle with a diameter of about 550μ,[5] whereas the original size of the particle was 700μ.

LASER SHADOWGRAPH AND PHOTOGRAPH RESULTS

Of the 20 firings in the program, 7 gave either laser shadowgraph or photographic data (Table II). Only the first round, C-1195, showed a complete symmetrical particle at the laser photograph station; the impact information indicates that some breakup may have occurred, but beyond the laser station.

Shadowgraphs were obtained for three rounds, C-1197, C-1202, and C-1211, from both the laser photographic station and the TBL shadowgraph station. In the last two of these, C-1202 and C-1211, particle breakup between the two laser stations was clearly indicated, for only one particle appeared in the laser photograph, whereas two appeared in the TBL laser shadowgraphs. (Streak data for C-1211 indicated two large particles also.) Furthermore, no clear impact information was obtained for C-1202, an indication that further breakup may have occurred.

Round C-1197 was particularly interesting because the breakup and loss of particles was evident in the laser shadowgraph (Fig. 22), where the main

particle is followed by four others ranging in size from about 50 μ to 100 μ. The separation distances shown in Figure 23 give some idea of the rapidity with which the smaller, secondary particles separate from the primary particle.

The particles shown in Figure 22 are evident in the laser photograph as small bright dots, such as those shown in Figure 24. Since the photographs of the particle were obtained with reflected light, a film with high sensitivity was needed. The film that was used, Polaroid Type 413, has a very large grain with a resolution of 20 — 30 lines/mm; consequently, data on particle shape had to be obtained from the higher-resolution film used in the shadowgraphs. (It is possible, however, to correlate the bright images on the photograph with the shadows in the shadowgraph obtained simultaneously.)

As expected, the increased heat input of rounds C-1195, 1196, and 1197, caused a successively greater breakup of the particles; and with a much higher range pressure than the first two, round C-1197 was in a greater state of disintegration at the laser station.

PARTICLE SHAPE DETERMINATION WITH THE ISODENSITRACER

The smear on a shadowgraph is a function of light duration and model velocity. Figure 25 shows the effect of smear on a record. The sides perpendicular to the line of flight of an object move in a straight line, but the front and rear surfaces smear to varying degrees, depending upon their position on the body. The object partly covers the smear of the front surface, so that the density gradient on the film is expected to be steeper for the front surface than for the rear surface. Although the steeper density gradient defines the front surface more clearly than the rear surface is defined, the degree of definition depends upon the light pulse. Duration of the light pulses for the two laser shadowgraph stations is shown in Figure 26.

Normal output for the laser photographic station is similar to that of the TBL laser. (Damage to the Nicol prism of the laser photograph station contributed to the spiked output shown.) The film response causes the effective smear on the film to be much less than the full 120 nsec; the laser station, as will be explained, shows an effective smear determined from the isodensitracer of about 25 to 35 nsec. The spiked output of the laser photograph station results in a series of smeared images, of which the most distinct, the one correlated with the first peak, is termed the principal image (Fig. 27). The other, secondary images can be correlated with succeeding maximums in the light impulse, and Figure 28 shows this time correlation for the rear of the front face of round C-1195. A similar time correlation for the isodensitrace of round C-1197 for the TBL is shown in Figure 29.

The isodensitrace[6] of the shadowgraph film resembles an ordinary isodensimeter trace, with the exception that instead of being just a record of film density levels along a given line, it is in two dimensions. Changes in density levels are indicated by a series of coded symbols consisting of blanks, dots, and lines. Figure 30, part of the data reduction of the isodensitrace for C-1195, plots density levels parallel and perpendicular to the line of flight, with the sides shown fairly well and the smear of the front and rear surface shown for the principal image. All isodensitraces showing a single particle were enlarged 50 times.

The velocity of the particle at the laser photograph station was 6.50 μ/nsec, and the length of the smear measured on the trace is 230 μ; this correlates exactly with the duration of the first light peak of 35 nsec. Figure 31, a similar plot for the TBL laser, shows an effective smear of 130 μ, with a corresponding light interval of 20 nsec. This again correlates with the light output shown in Figure 26.

The shape determined from the isodensity record of round C-1196 indicates particle breakup (Fig. 32). Particles were also evident in the wake of the

object in the shadowgraph. In a comparison of profiles from the bow to the stern of the records for C-1195 and C-1196, the loss of fragments from C-1196 is clearly evident (Fig. 33), and the shape of the particle determined from this trace (Fig. 35) is characteristic of a material undergoing mechanical breakup. Round C-1209 showed the same type of shape. In Figure 35, an enlargement of the actual shadowgraph and the shape of the particle determined from the isodensity record, the primary image and the slight darkening in front of the primary image from the secondary images are both clear.

Figures 36 and 37 show the two particles evident at the TBL laser station for C-1202 and C-1197; the relative sizes of the particles can be seen easily in the isodensity records. Figures 38, 39, and 40 show the particle shapes determined for rounds C-1202, 1210, and 1211 — all indicate particle breakup. Although the shadowgraph of C-1210 and the TBL shadowgraph of C-1211 appear to be slightly out of focus, the break of the primary particle into two large pieces is clear in C-1211, and the ragged outline of the particle in C-1210. The small size of the particle (400μ) in round C-1210 makes the record even more difficult to evaluate than the others.

DISCUSSION OF RESULTS

The mechanical breakup of the Al_2O_3 during flight can be attributed to the thermal stresses induced in the sphere by the temperature gradient in the particle. If the surface is uniformly heated to the melting temperature, an analysis given by Timoshenko[7] can be used to calculate the level of induced thermal stress.

If the surface temperature is assumed to be melt temperature, the maximum tension induced in the sphere is given by

$$\sigma_t = k_1 \frac{\alpha E}{2(1-\nu)} (T_m - T_o)$$

where

T_m = melt temperature

T_o = initial temperature

α = temperature coefficient of expansion

E = elasticity modules

ν = Poisson's ratio

k_1 = a constant approaching 1

Based on this calculation,

$$\sigma_t \approx 400,000 \text{ psi}$$

Even a slow heat input raising the temperature gradually (leaving, for example, a $1000^{o}F$ difference between the center of the sphere and the surface) would still give a stress level of about

$$\sigma_t \approx 120,000 \text{ psi} \qquad \Delta T = T_m - T_o = 1000^{o}F$$

With a maximum tensile strength of approximately 40,000 psi, alumina is a brittle material that would not be expected to yield at high levels of stress. Although the stress calculations may be refined by consideration of the computer-predicted temperature profiles and a more detailed analysis, this is probably not warranted since estimates of the order of the thermal stress are considerably larger than the maximum tensile stress of the material. A slight rotation of spheres in flight could give a more or less symmetrical temperature distribution, thus the assumption that the temperature field is symmetric may not limit the analysis seriously.

A low thermal diffusitivity of Al_2O_3 limits the initial temperature penetration to a thin layer on the surface. Since an analysis of a thin layer gives essentially the same stress levels as previously calculated,[7] mechanical degradation of the particles during flight might be expected to occur, causing layers of the

particle to flake off, before the formation of a melt layer. Being crystal, Al_2O_3 might break along preferred crystalline planes; the launch attitude itself might therefore have some effect on the eventual disintegration of the sphere.

CONCLUSIONS

This study demonstrated that it is possible to launch and measure the velocity of individual spheres (diameter 400 to 700 microns) traveling at velocities of 7 to 8 km/sec in air. It was also demonstrated that it is possible to obtain definitive laser shadowgraphs of spheres traveling at these velocities.

The experimental results showed that mechanical breakup, or disintegration, of the particles occurred during flight. Considerations of thermal stress levels in the particles and the brittleness of Al_2O_3 would indicate that at the velocities and free stream conditions and used in this study the particles should be expected to break up in flight.

SUGGESTIONS FOR FUTURE WORK

Launching models in a light-gas gun produces accelerations as high as 2×10^6g. Despite this high acceleration load, the very small weight of the particles keeps stress levels in the particles well below the strength of the material. These levels, however, have the nature of a shock loading, with the possibility that crystalline planes in the models might fracture in the launch process. Thus, although the experiments indicate that thermal stress levels in the particles are the cause of their breakup, a series of tests should be made to eliminate the launch process as one of the possible factors in particle breakup. A short program involving flight conditions with low heat input, with laser photographs and shadowgraphs at the muzzle, would give a definitive answer.

A continuation of the program, using a longer range, smaller particle sizes, and lower range pressures, would also be advisable. (Pressures from 5 to 10mm of Hg, with a range of 150 ft and particles to 200μ, could be obtained in future tests.)

Finally, a program based on a yielding material, such as gold or platinum, could be conducted. The results of feasibility tests indicate that with a 10-nsec laser and some improvements in the optics of the shadowgraph stations, shape changes of 30μ to 40μ could be determined. And if liquid droplets were to form in the wake, particle size down to about 15μ to 20μ could be distinguished.

REFERENCES

1. Collins, D.J., and Sangster, D.K., "Parametric Studies of a Fixed Geometry Light-Gas Gun," GM DRL TR66-01H, General Motors Corporation, Santa Barbara, Calif., Jun 1966

2. Anderson, C.B., "Thermal Response of Charring Ablator Heat Protection Systems Programmed for the IBM 7094 Digital Computer," Aerospace Corporation TOR-669 (S6855-20)-3, Feb 1966

3. Goldsmith, A., et al, Handbook of Thermophysical Properties of Solid Materials, Rev. ed., Volume III Ceramics, Macmillan Co., New York, 1961

4. Matula, R.A., "Comparison between Exact and One-Dimensional Theories for Incipient Melting in Reentry Simulation," ASME Preprint 62WA/HT53

5. Christman, D.R., "Target Strength and Hypervelocity Impact," Vol. 4 No. 10 AIAA, Oct 1966, p. 1872

6. Miller, Carlton S., et al, "Simplified Two-Dimensional Microdensitometry," Nature, Vol. 202, No. 4938, Jun 1964, pp. 1196 — 1200

7. Timoshenko, S., and Goodier, J.H., Theory of Elasticity, Second ed., McGraw-Hill 1951, pp. 416 — 421

Table I

SUMMARY TABLE OF ALL ROUNDS

Round No.	Model Mass (mg)	Model Diam. (microns)	Chamber Pressure (mm Hg)	Launch Velocity (m/msec)	Launch Weight (g)	Impact Comments
1185	.72	700	25	7.65	.44122	
1186	.72	700	25	7.83	.43742	1 Large Crater, 5 small
1190	.72	700	25		.43812	1 Large Crater, 5 small
1191	.72	700	25	7.80	.44032	Foil, 1 Large Crater, 2 small
1192	.72	700	25		.44602	Foil, 1 Large Crater, 2 small
1193	.72	700	25		.44672	
1194	.72	700	25		.45612	
1195	.72	700	25	7.21	.45332	Foil Destroyed, 1 Large Crater, 1 small
1196	.72	700	25	7.28	.45602	Foil, 1 Large Crater, many small
1197	.72	700	50	7.16	.47802	Block, 1 Large Crater, Clean
1200	.72	700	50	7.27	.45102	Block, 1 Large Crater, 1 small
1201	.72	700	40		.42142	Block, 1 Large Crater, 1 medium and 1 small
1202	.26	500	25	7.77	.45036	Few small craters
1203	.26	500	25		.44116	
1204	.26	500	15		.45526	1 Large crater
1205	.13	400	20		.44683	
1207	.13	400	20		.44203	
1209	.26	500	25	7.77	.44266	Good Data, 1 Crater
1210	.13	400	25	7.91	.44133	
1211	.26	500	35	(7.73)	.4499	

Table II

VELOCITY DATA SUCCESSFUL ROUNDS

Round No.	Model Mass (mg.)	Model Diam. (microns)	Chamber Pressure (mm Hg)	VELOCITY (m/msec) Launch	Laser Schlieren	Laser Photograph	TBL Laser Shadowgraph	Impact
1195	.72	700	25	7.21	6.70	6.50	6.29	6.10
1196	.72	700	25	7.28	6.77	6.58	6.37	6.17
1197	.72	700	50	7.16	6.38	6.10	5.82	5.52
1202	.26	500	25	7.77	7.00	6.72	6.46	6.13
1209	.26	500	25	7.77	7.00	6.72	6.46	6.13
1210	.13	400	25	7.91	6.96	6.63	6.30	5.97
1211	.26	500	35	7.73	6.70	6.34	5.99	5.64

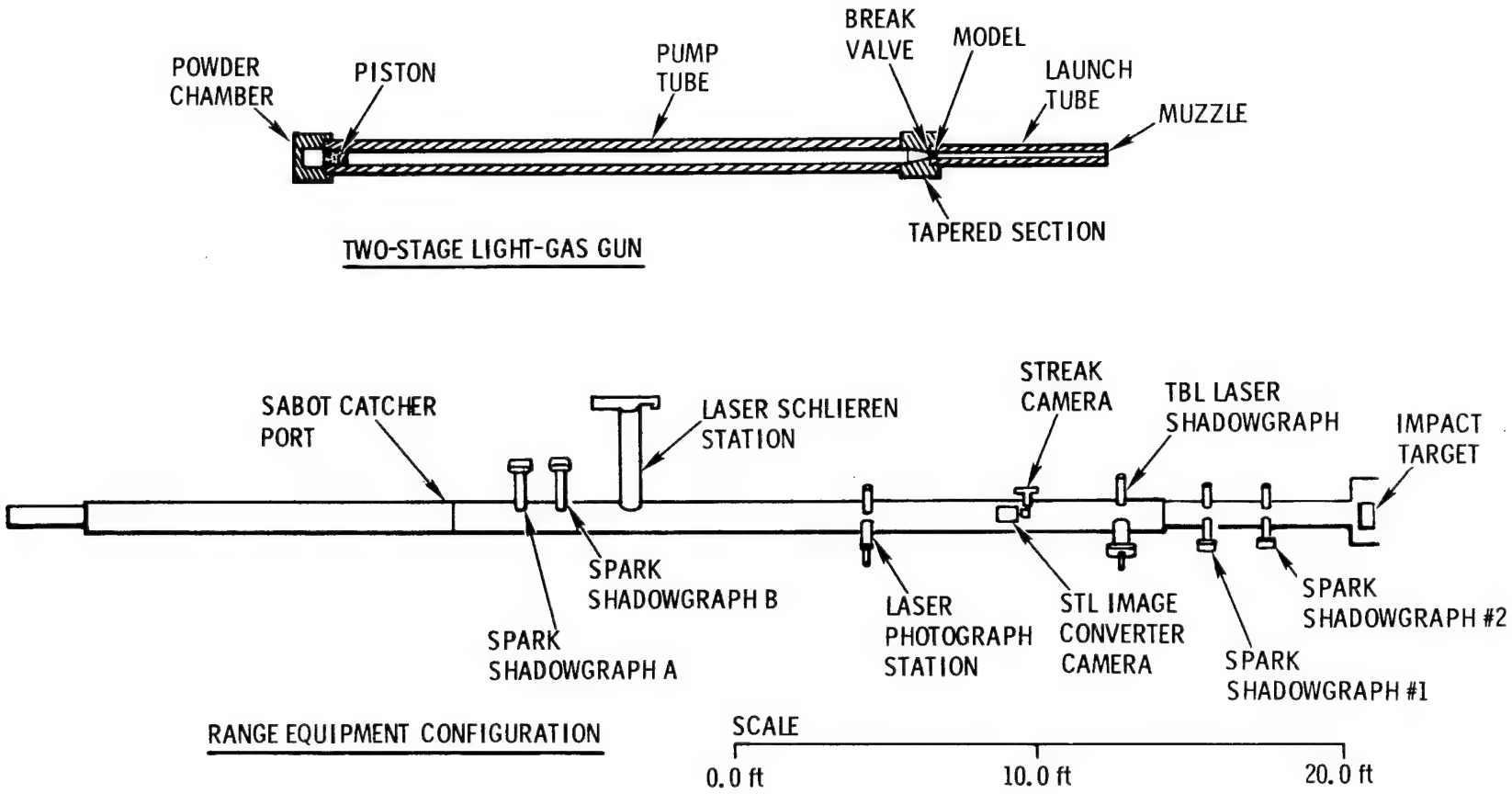

Figure 1 Range Configuration

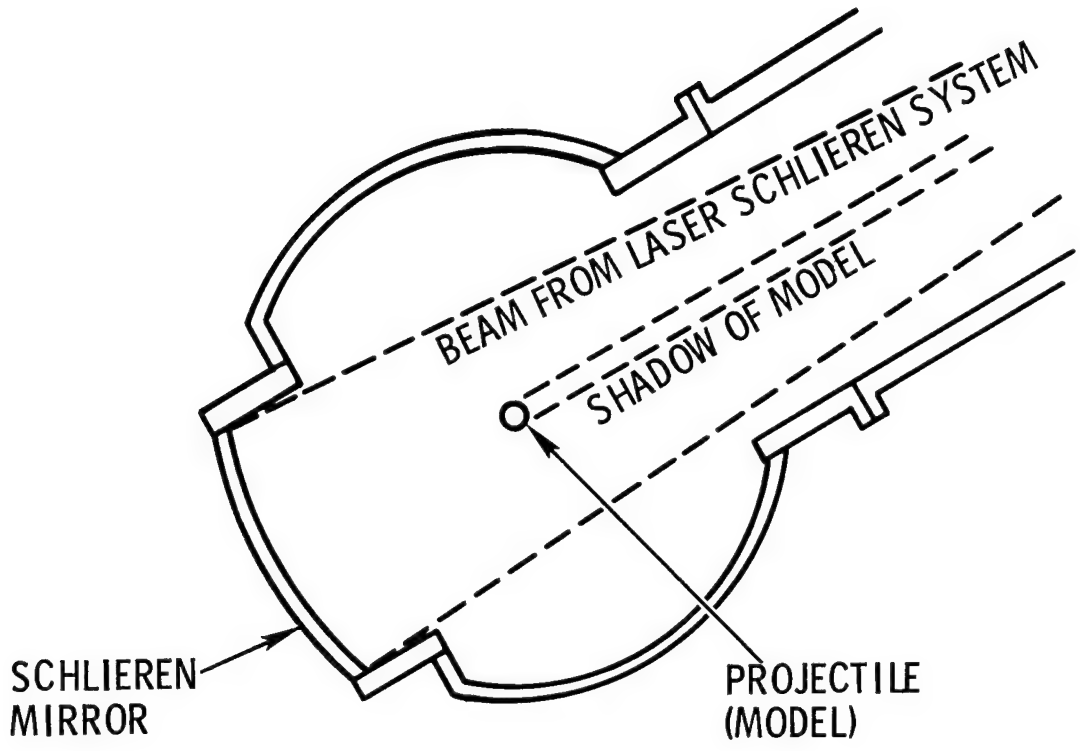

Figure 2 Schematic Laser Schlieren

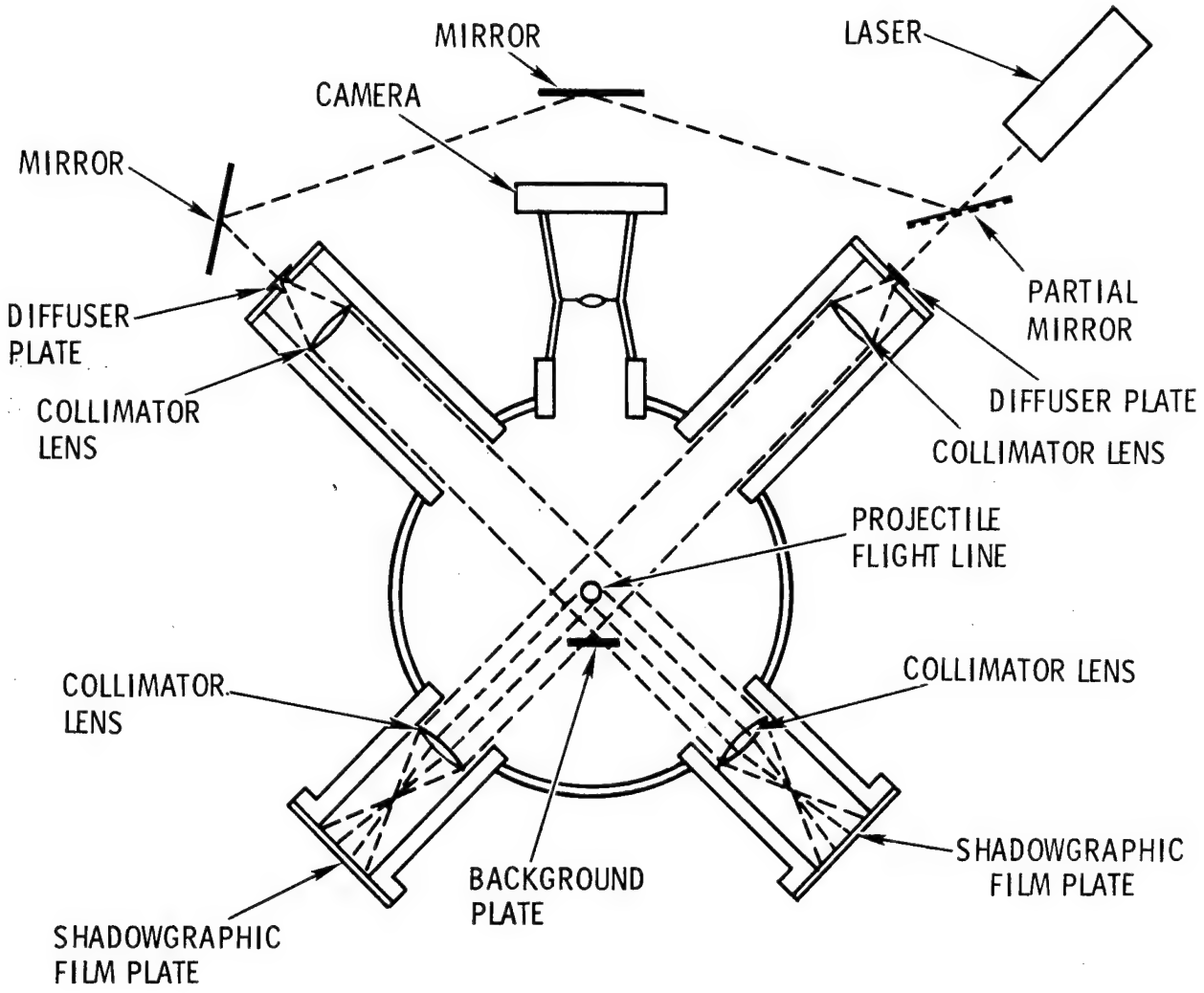

Figure 3 Schematic Laser Photograph and Shadowgraph Station

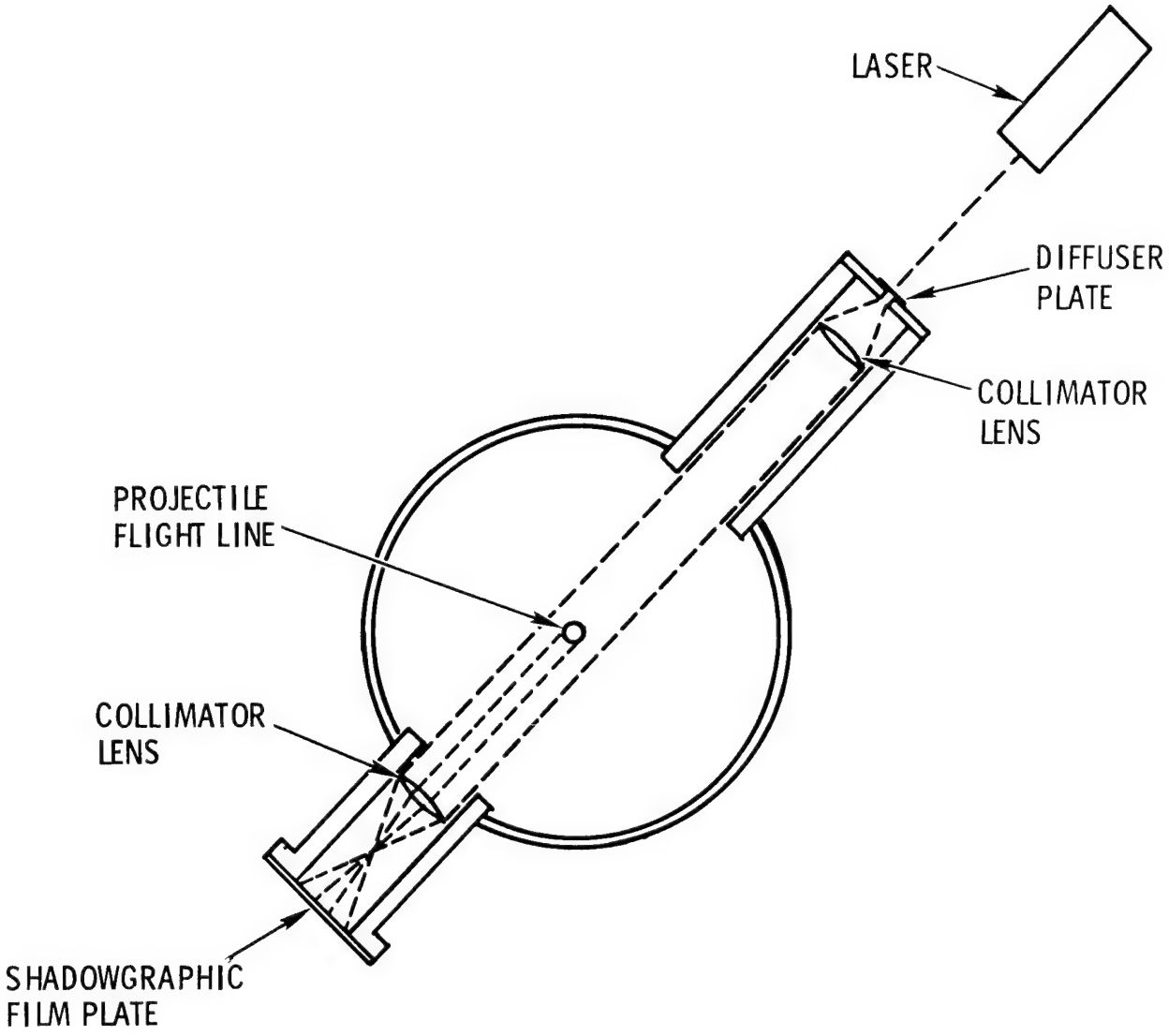

Figure 4 Schematic Laser Shadowgraph (TBL)

THERMOPHYSICAL PROPERTIES OF Al_2O_3

Density	4.0 g/cm^3
Melting Point	2308°K
Heat of Sublimation	4473 cal/g at 298°K 1472 cal/g at 2223°K
Specific Heat	.19 cal/g °K at 298°K .31 cal/g °K at 1500°K
Thermal Conductivity	.082 cal/sec cm °K at 298°K .015 cal/sec cm °K at 1500°K

MECHANICAL PROPERTIES

Coefficient of Thermal Expansion	4.3×10^{-6} per °F
Modulus of Elasticity in Tension	3.45×10^6 bars
Tensile Strength	2680 bars
Poisson's Ratio	~0.25

Figure 5 Material Properties of Al_2O_3

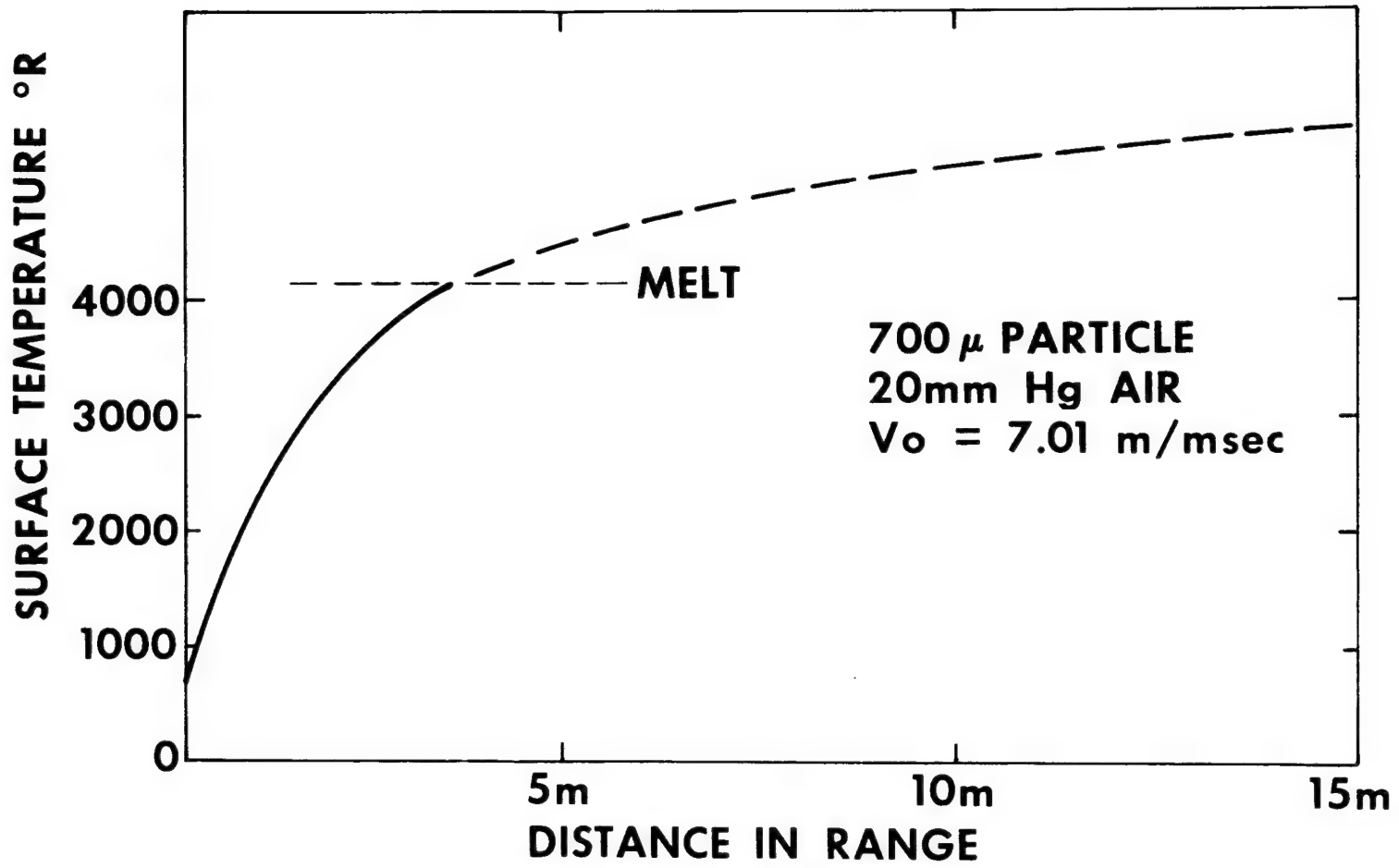

Figure 6 Surface Temperature as a Function of Range Distance

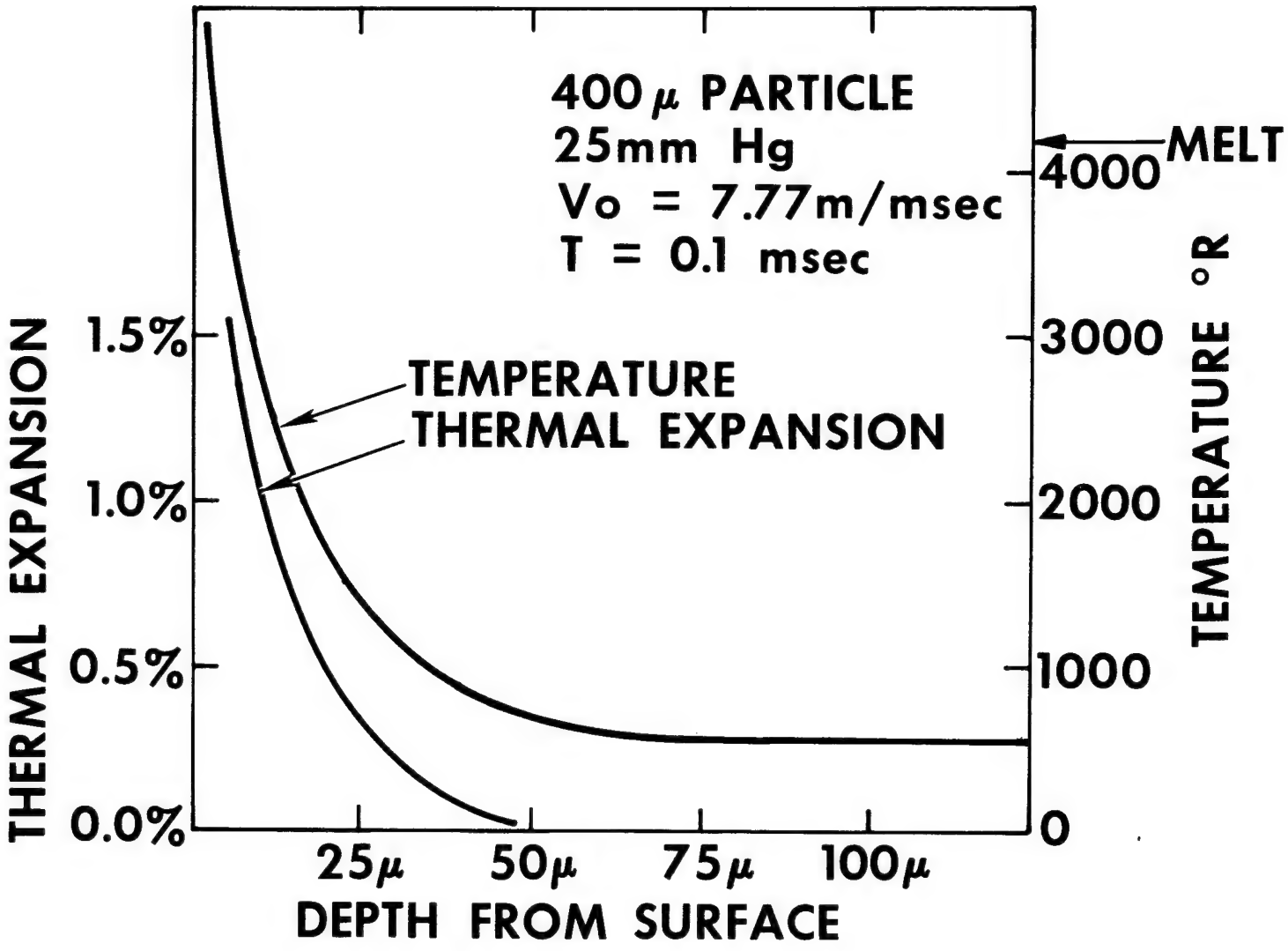

Figure 7 Temperature Gradient and Thermal Expansion in Bow of Model

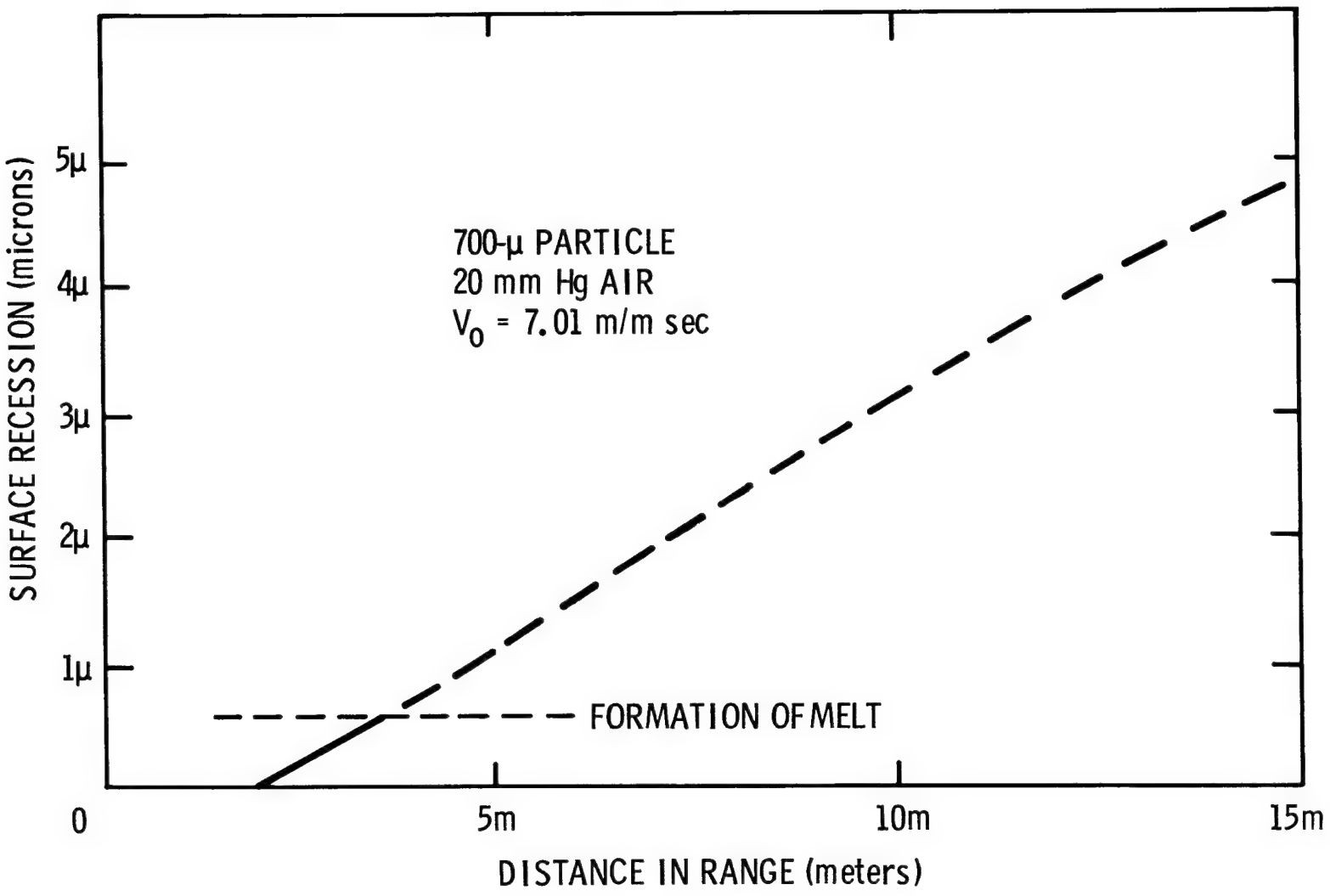

Figure 8 Surface Recession Rate as Function of Range Distance

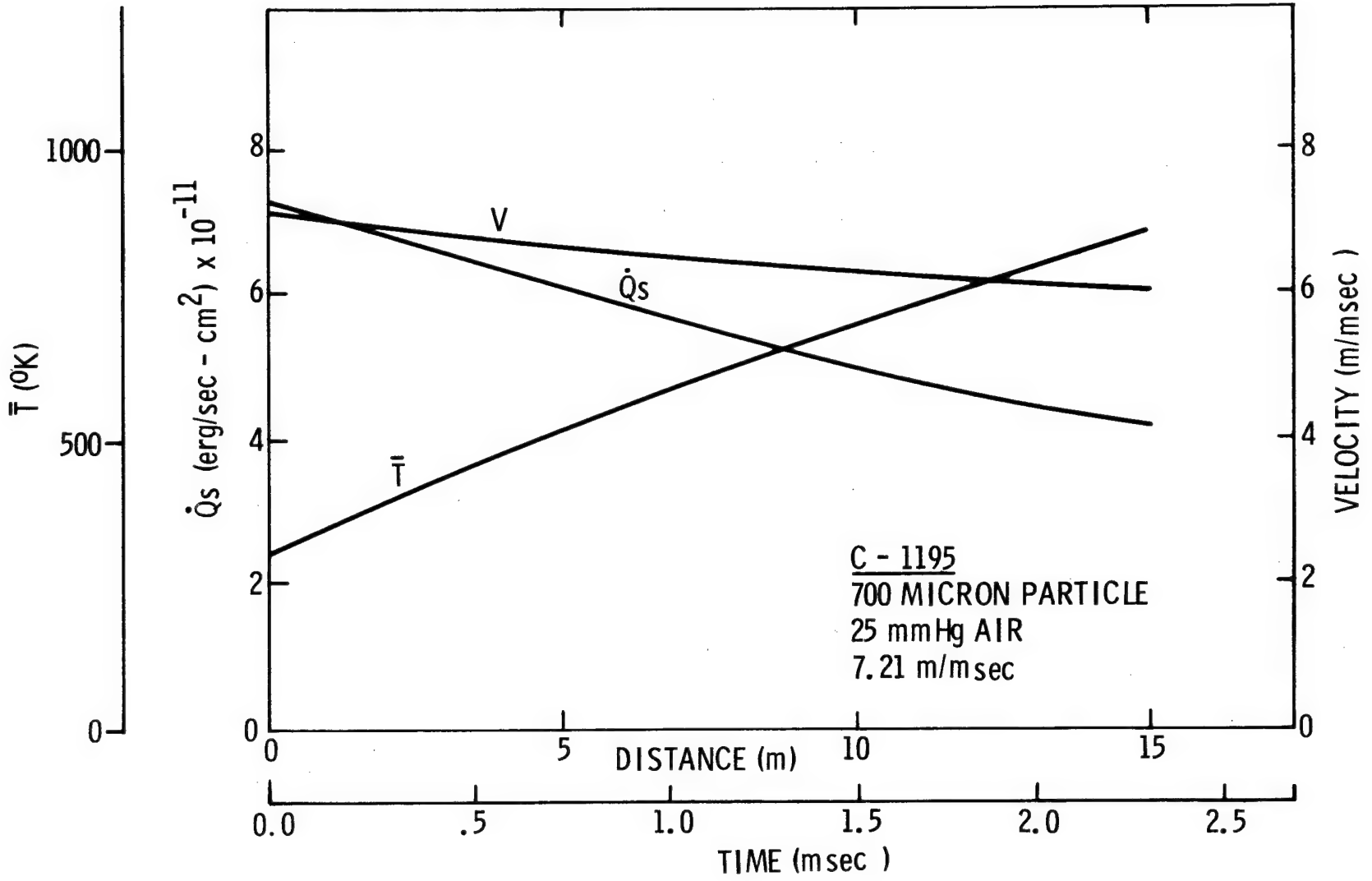

Figure 9 Velocity, Heat Input, and Mean Temperature Curves for Data Rounds

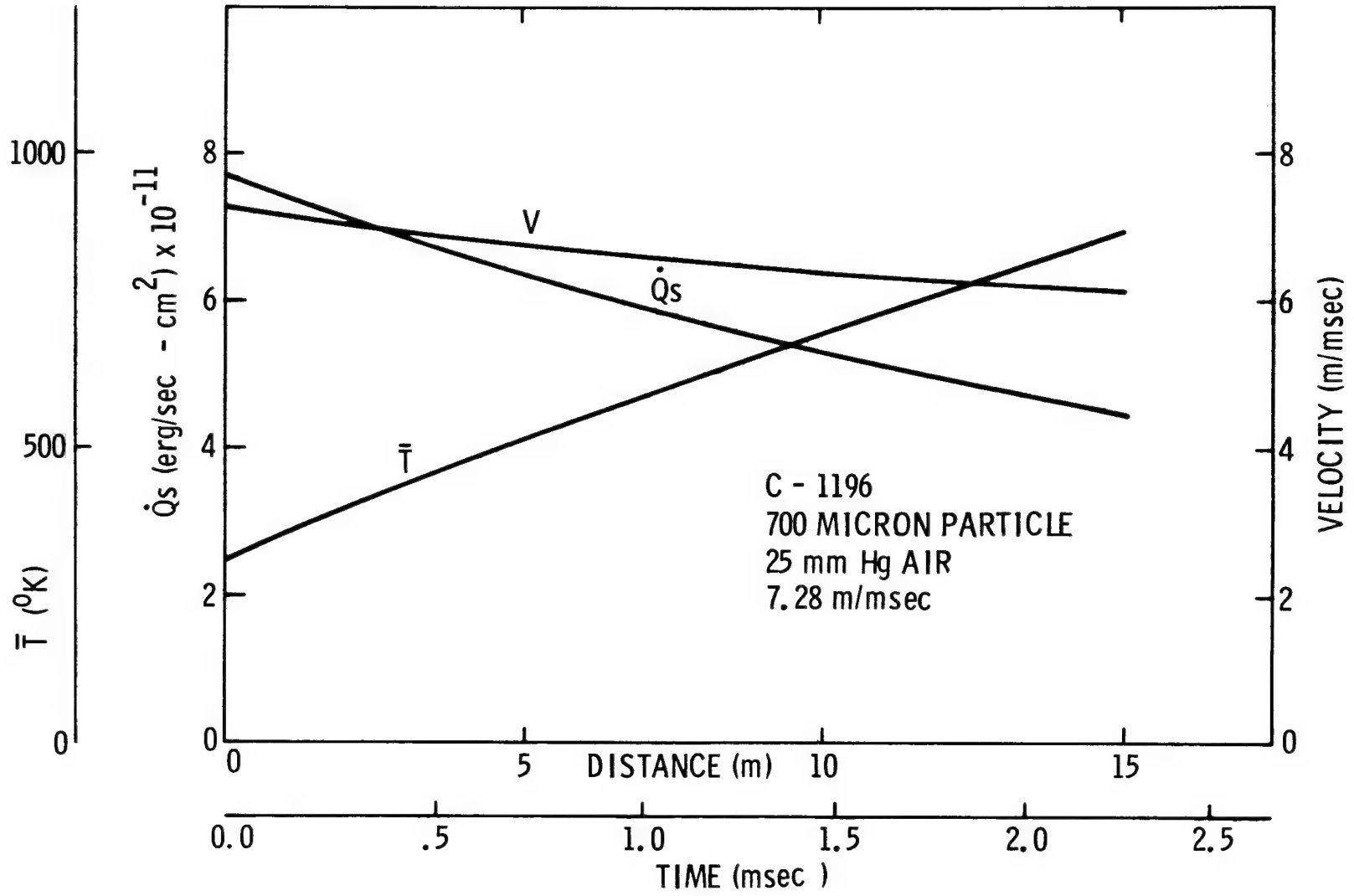

Figure 10 Velocity, Heat Input, and Mean Temperature Curves for Data Rounds

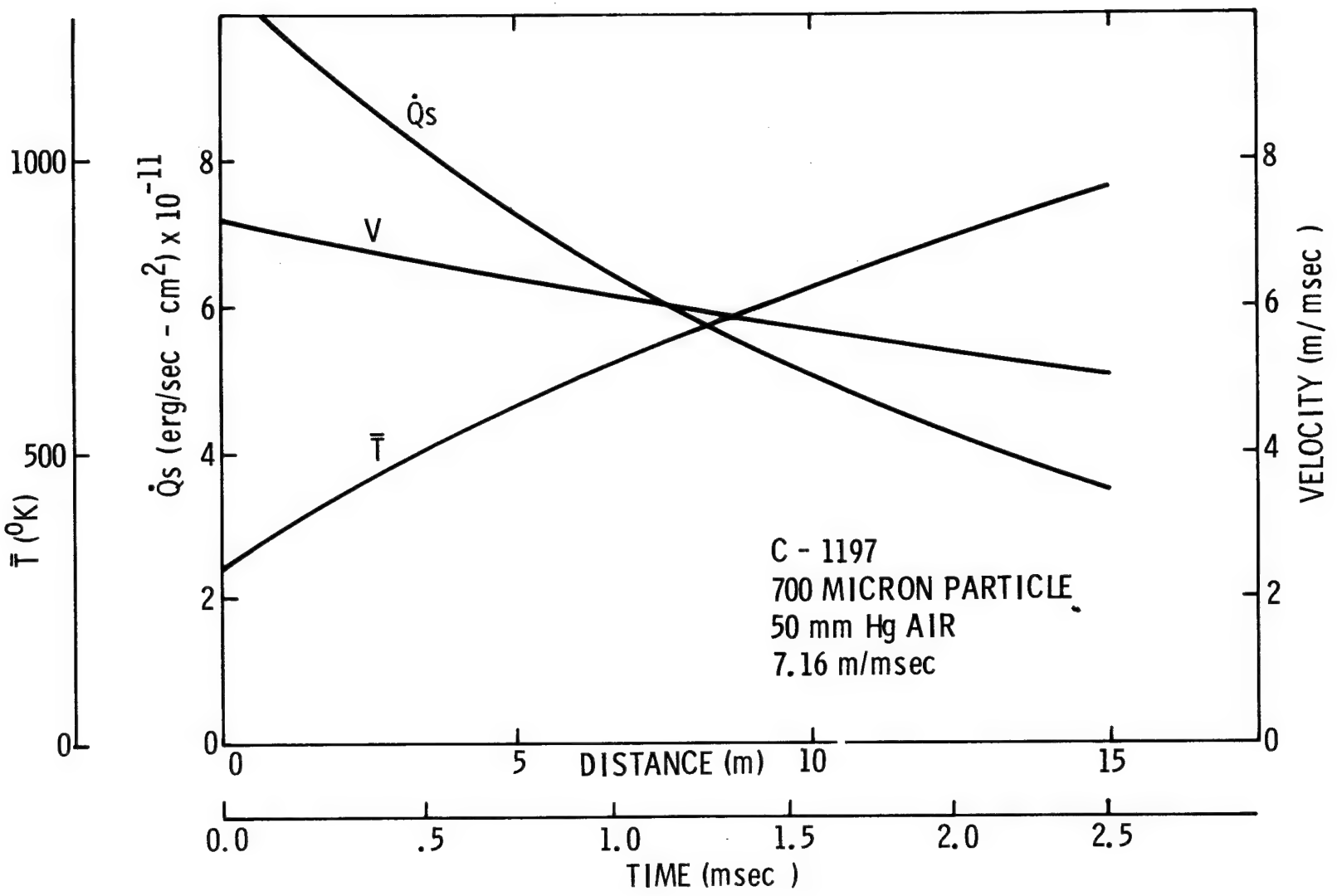

Figure 11 Velocity, Heat Input, and Mean Temperature Curves for Data Rounds

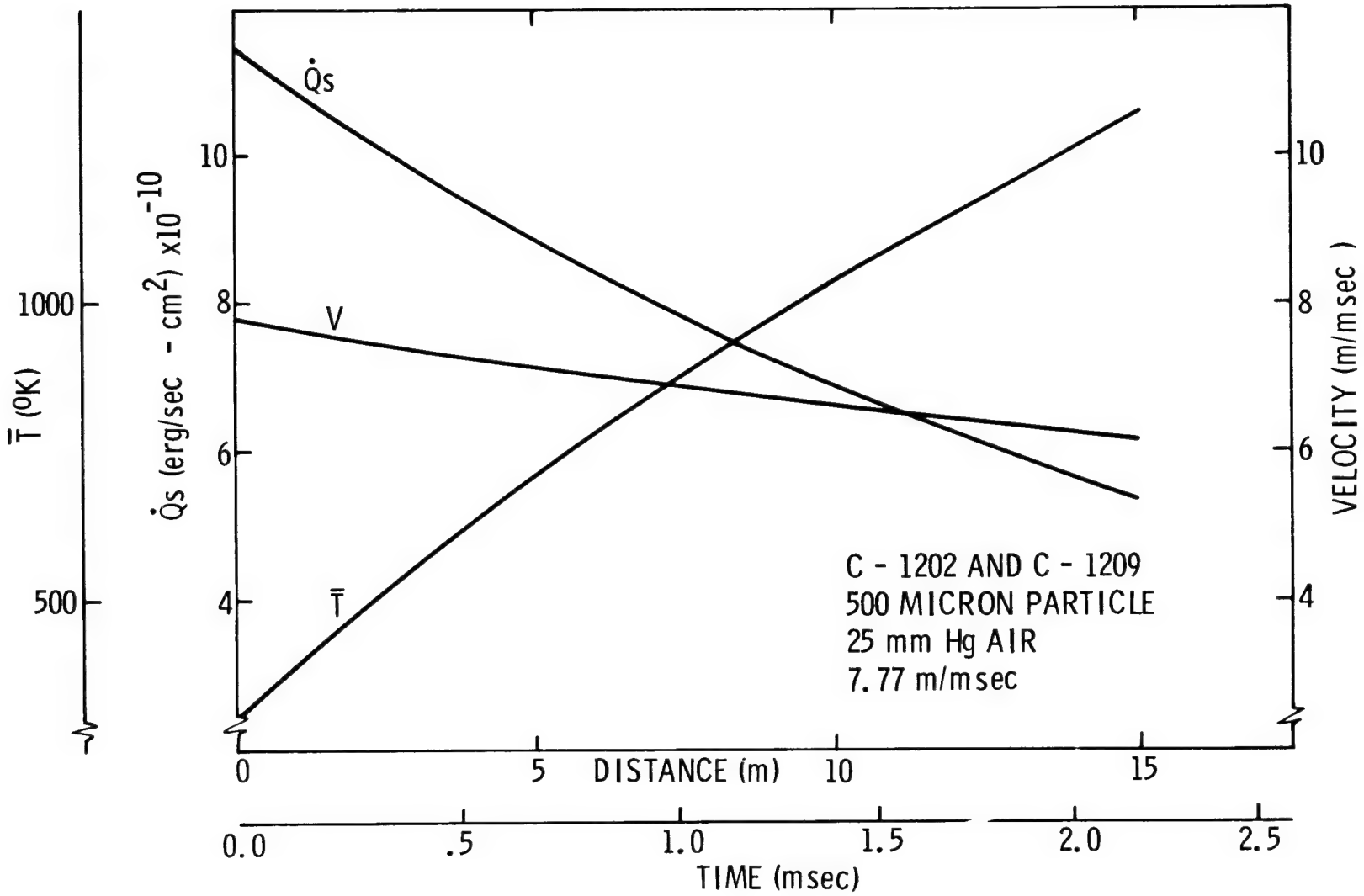

Figure 12 Velocity, Heat Input, and Mean Temperature Curves for Data Rounds

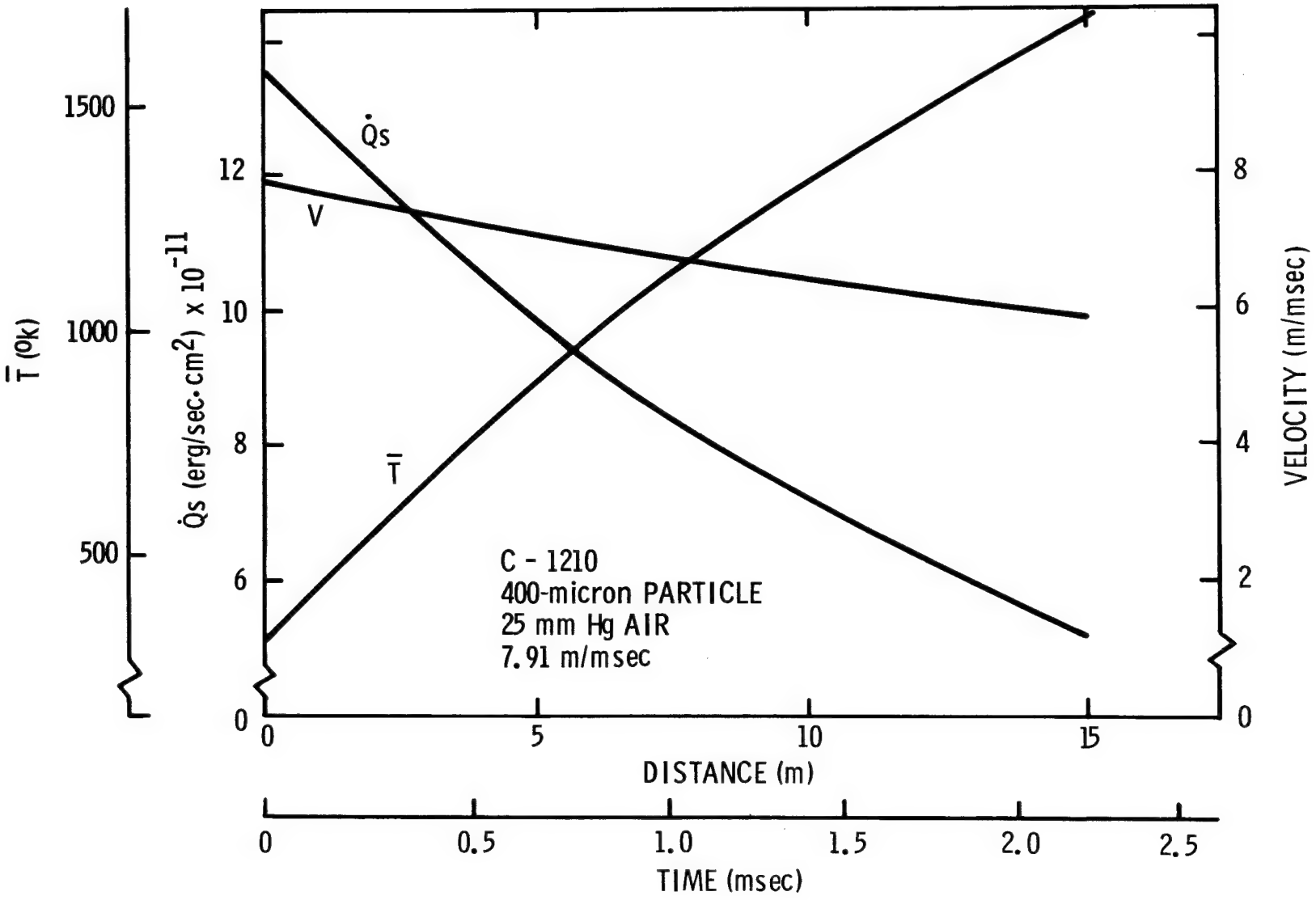

Figure 13 Velocity, Heat Input, and Mean Temperature Curves for Data Rounds

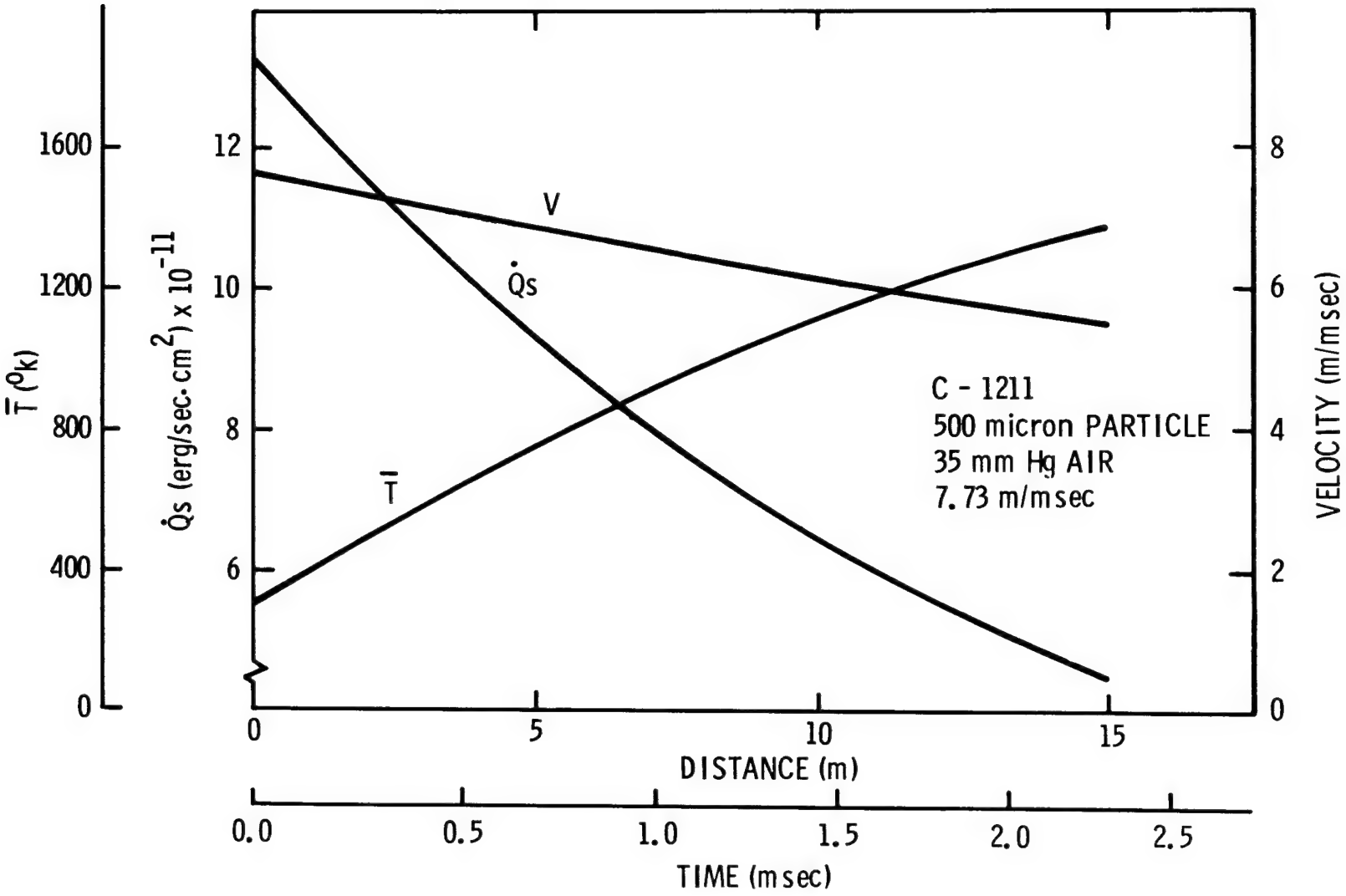

Figure 14 Velocity, Heat Input, and Mean Temperature Curves for Data Rounds

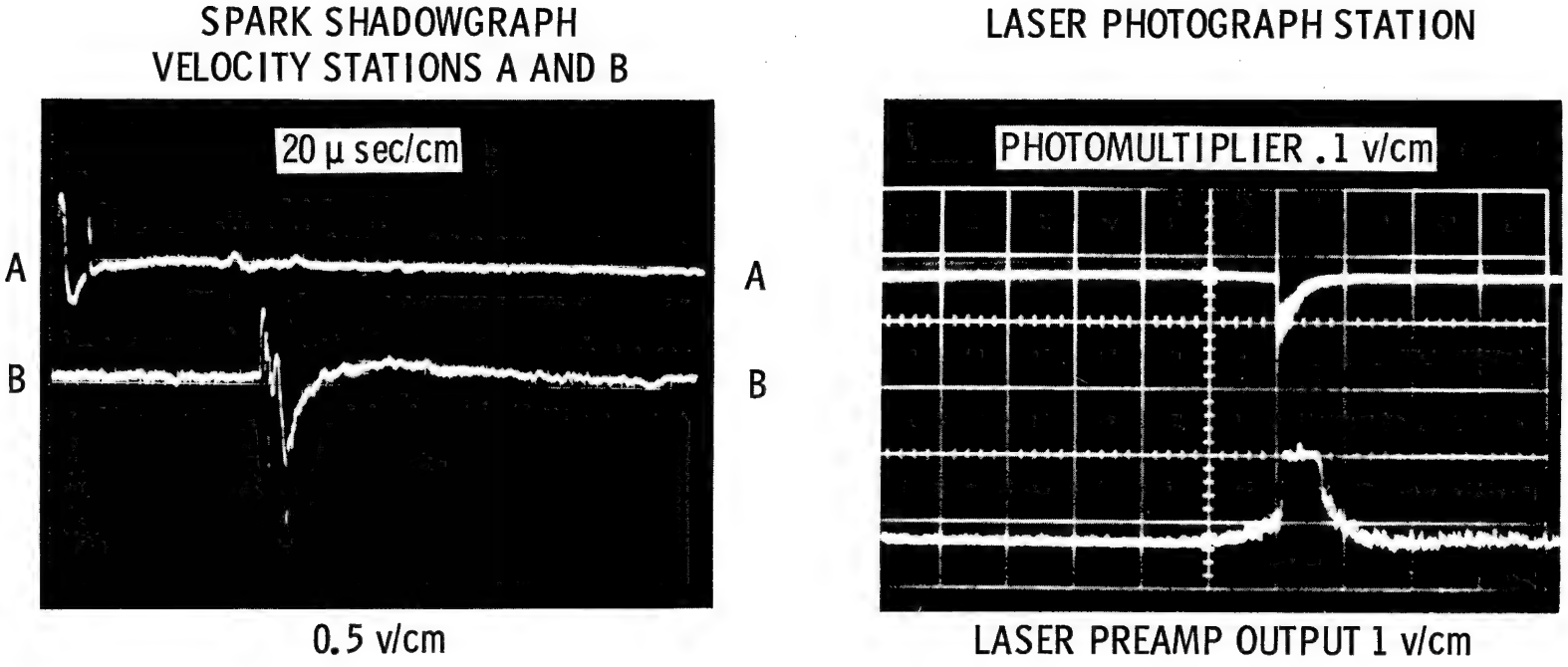

Figure 15 Typical Trigger Signals for Instrumentation

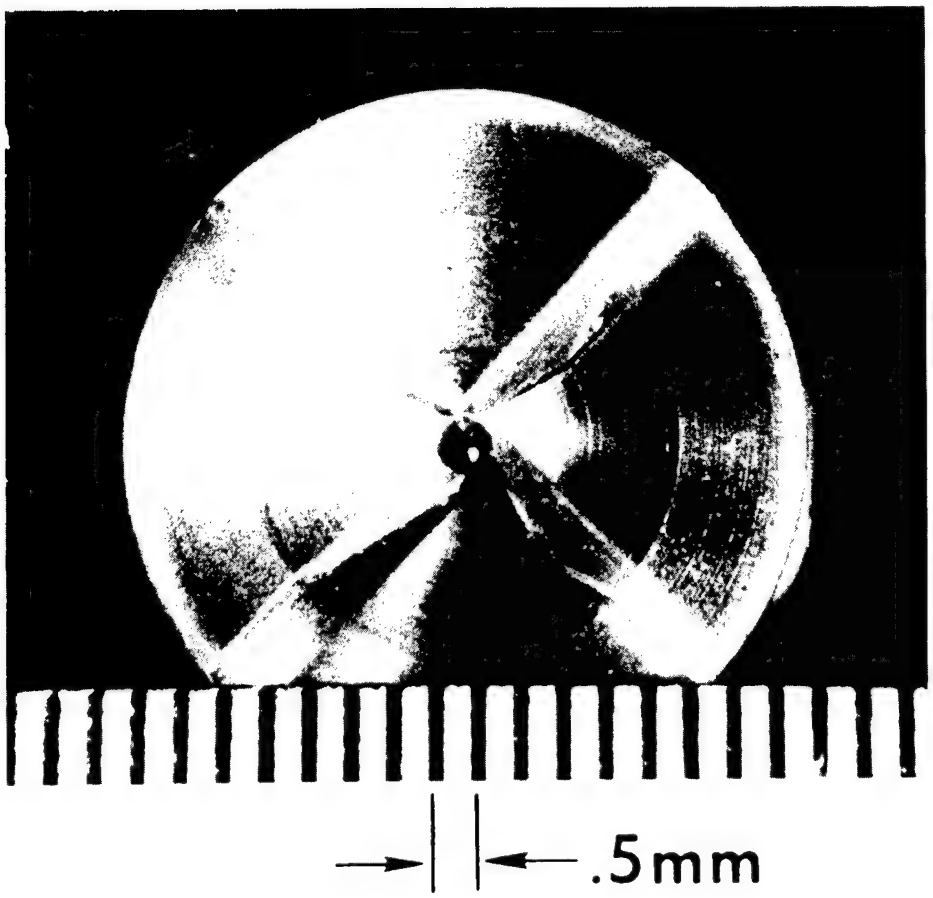

Figure 16 Front View of Sabot and Model (700μ Al_2O_3)

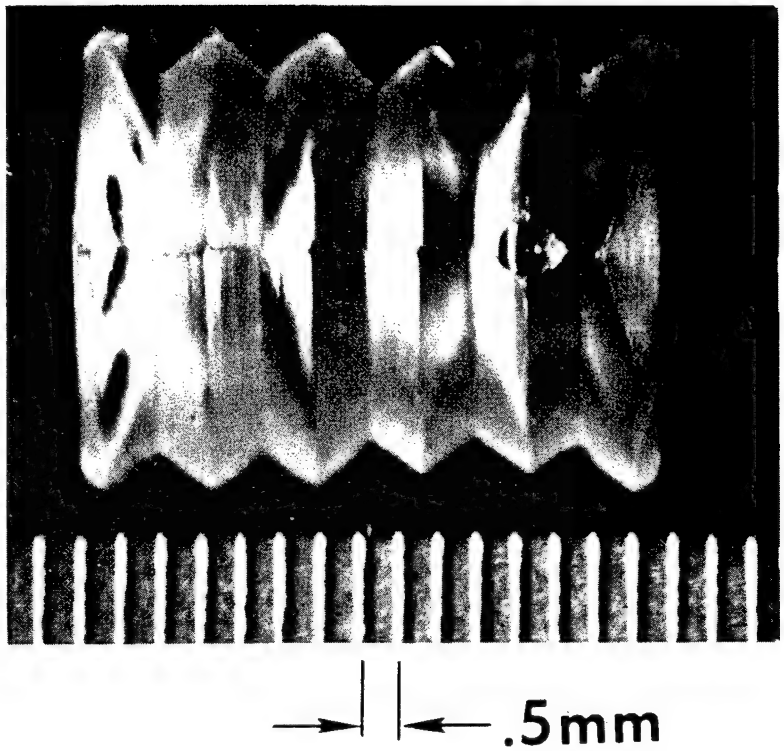

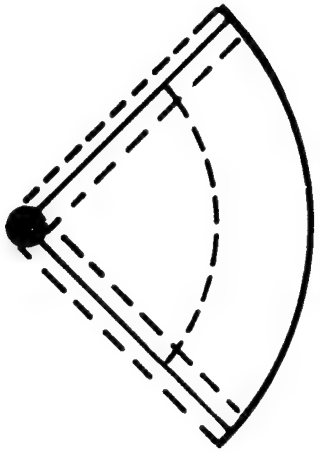

Figure 17 Segmented View of Sabot and Model (700μ Al_2O_3)

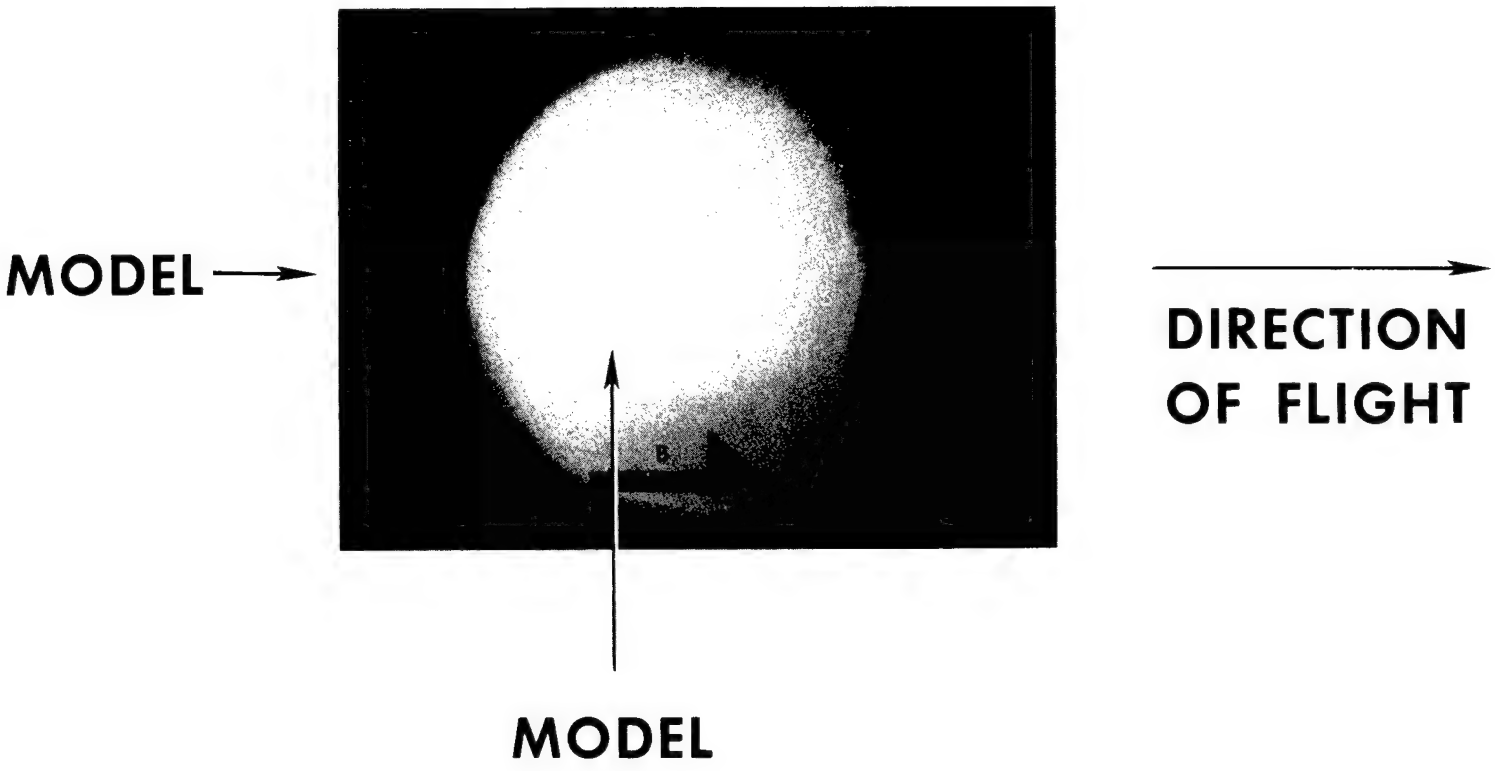

Figure 18 Typical Spark Shadowgraph

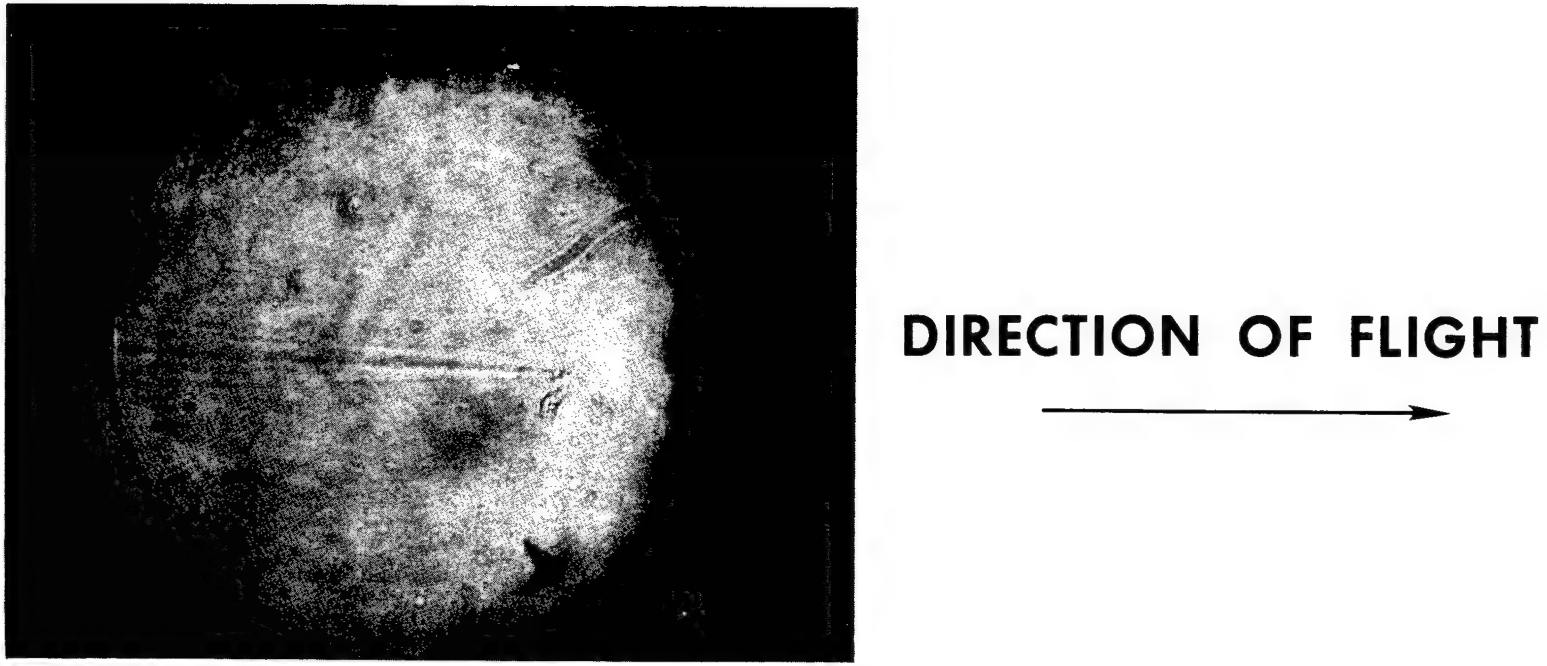

Figure 19 Typical Laser Schlieren

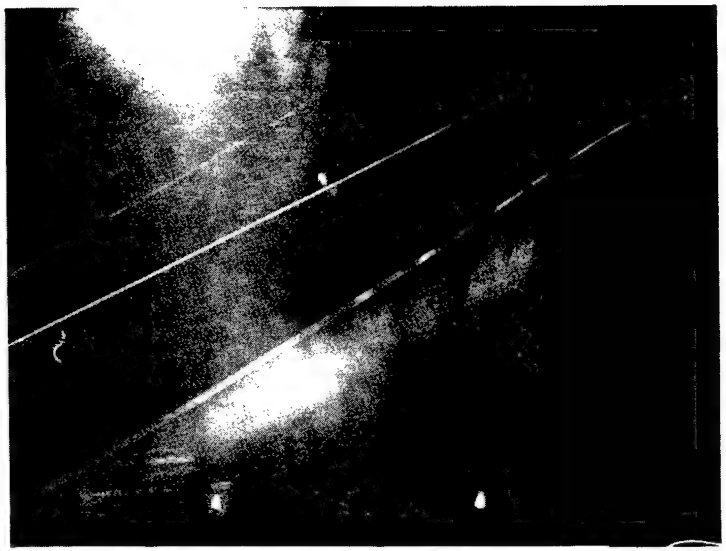

C-1196

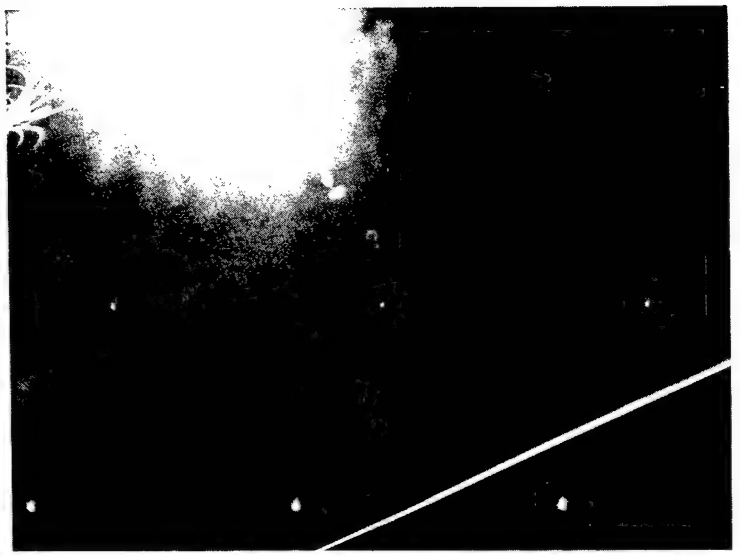

C-1197

Figure 20 Streak Pictures

C-1209

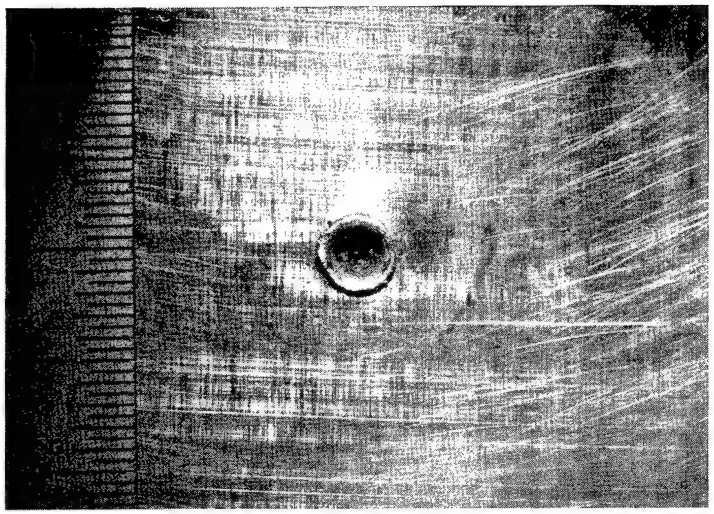

C-1186

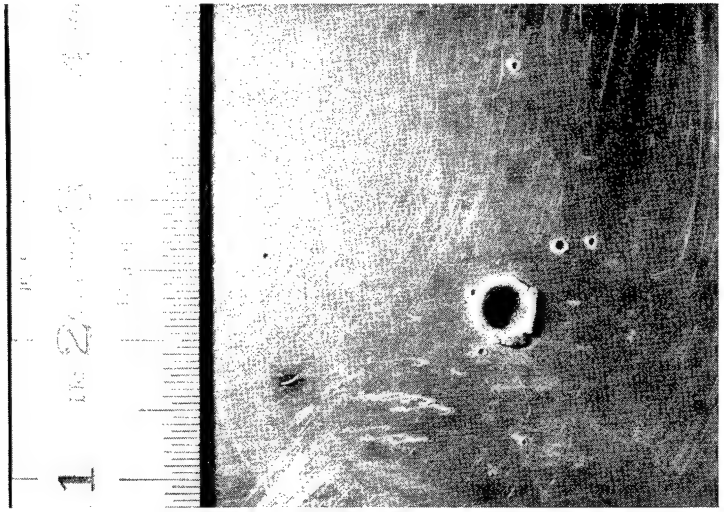

Figure 21 Impact Pictures

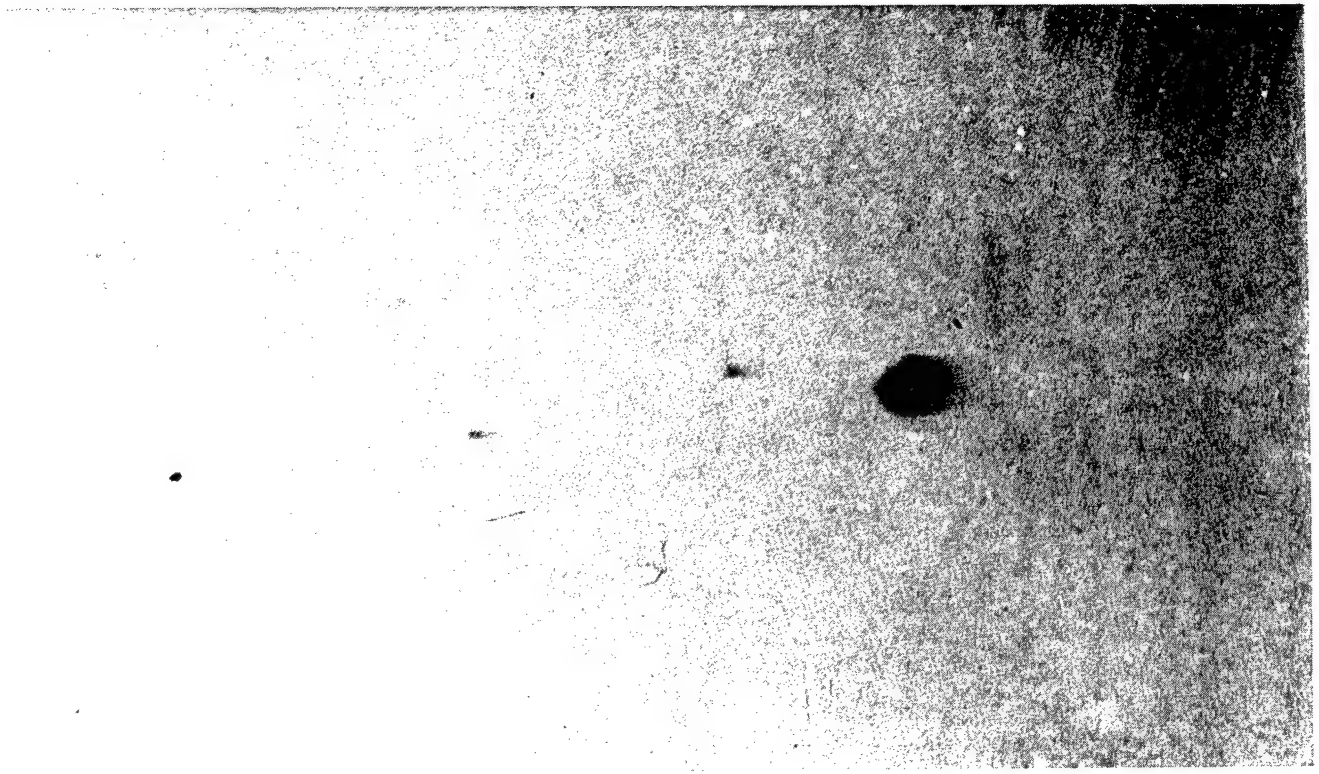

DIRECTION OF FLIGHT ⟶

Figure 22 Partical Breakup in Flight, Round C-1197

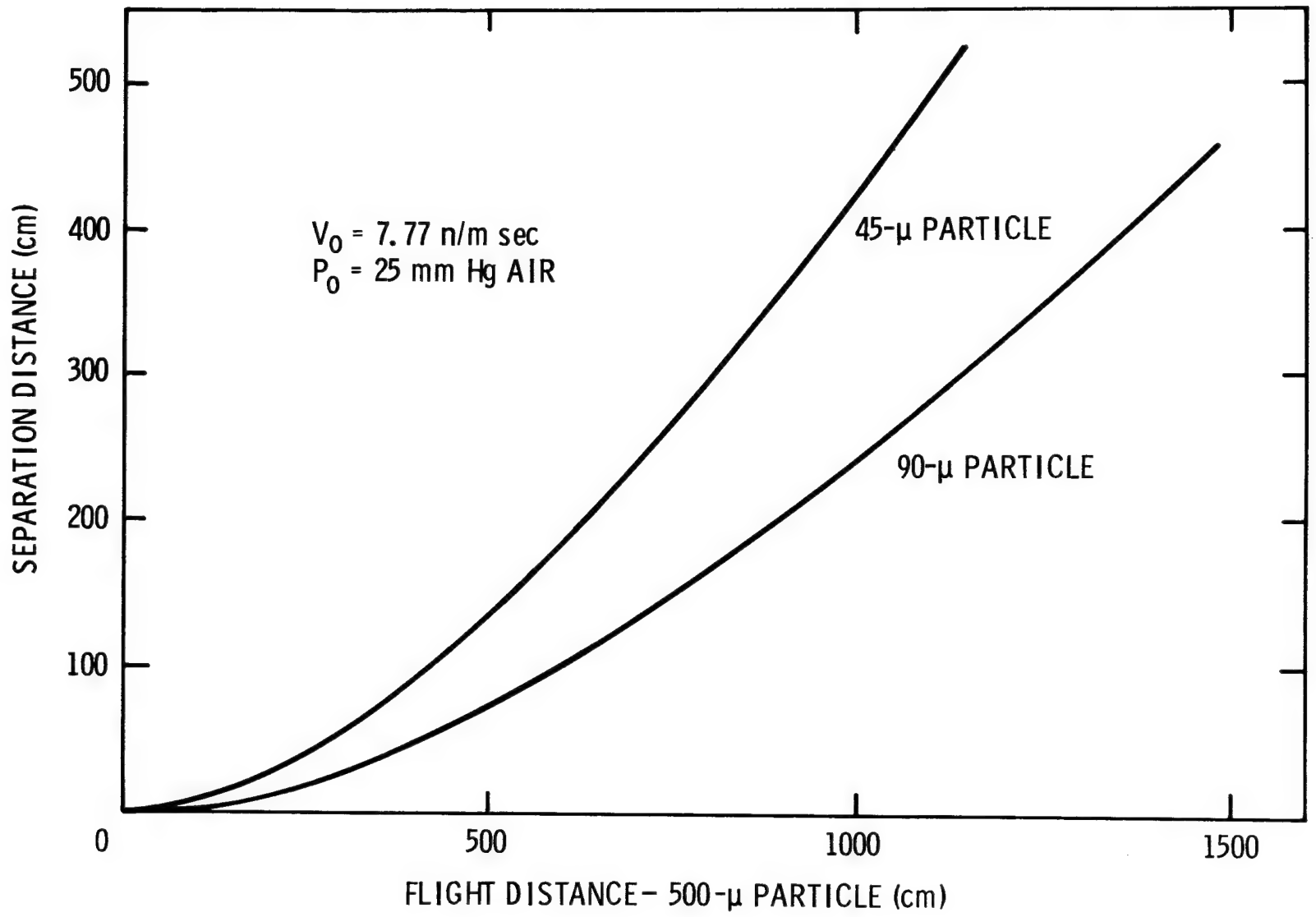

Figure 23 Separation Distance of Primary and Secondary Particles vs Flight Distance

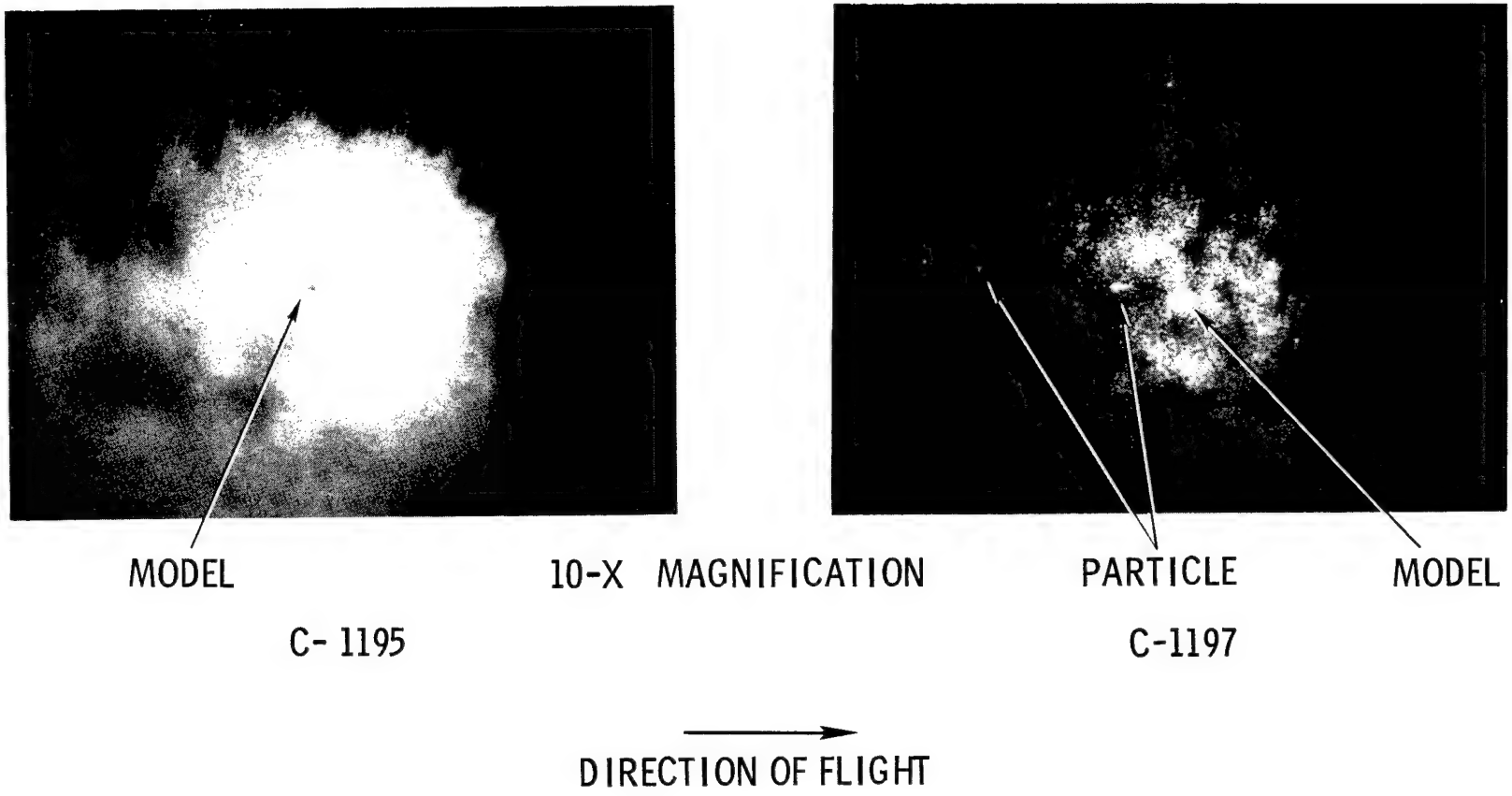

Figure 24 Typical Laser Direct Photographs

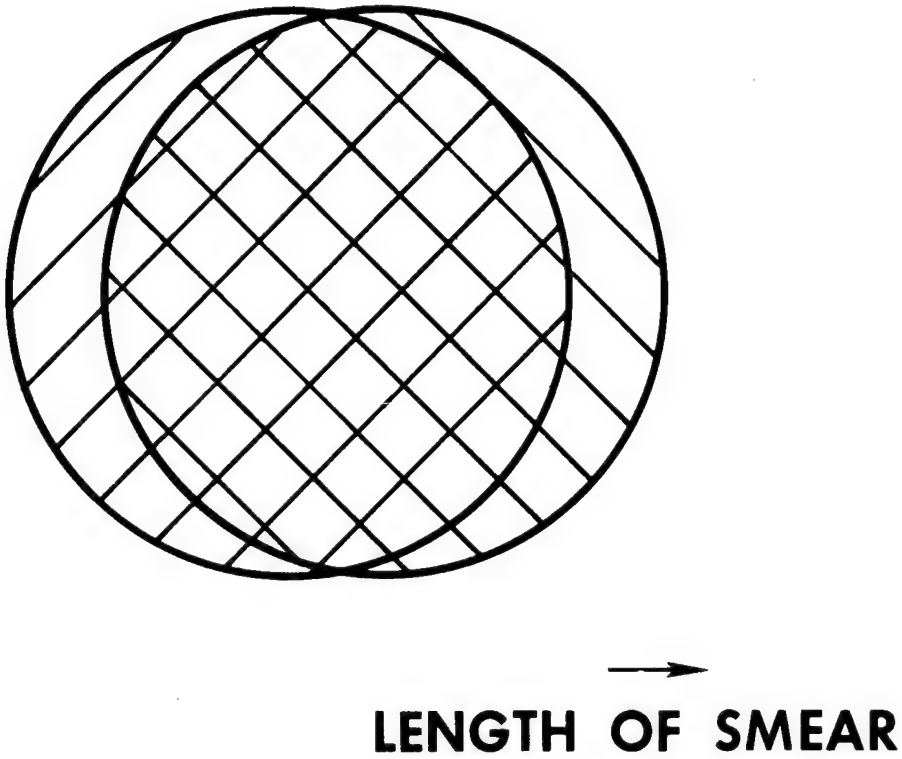

Figure 25 Effect of Smear on Film Records

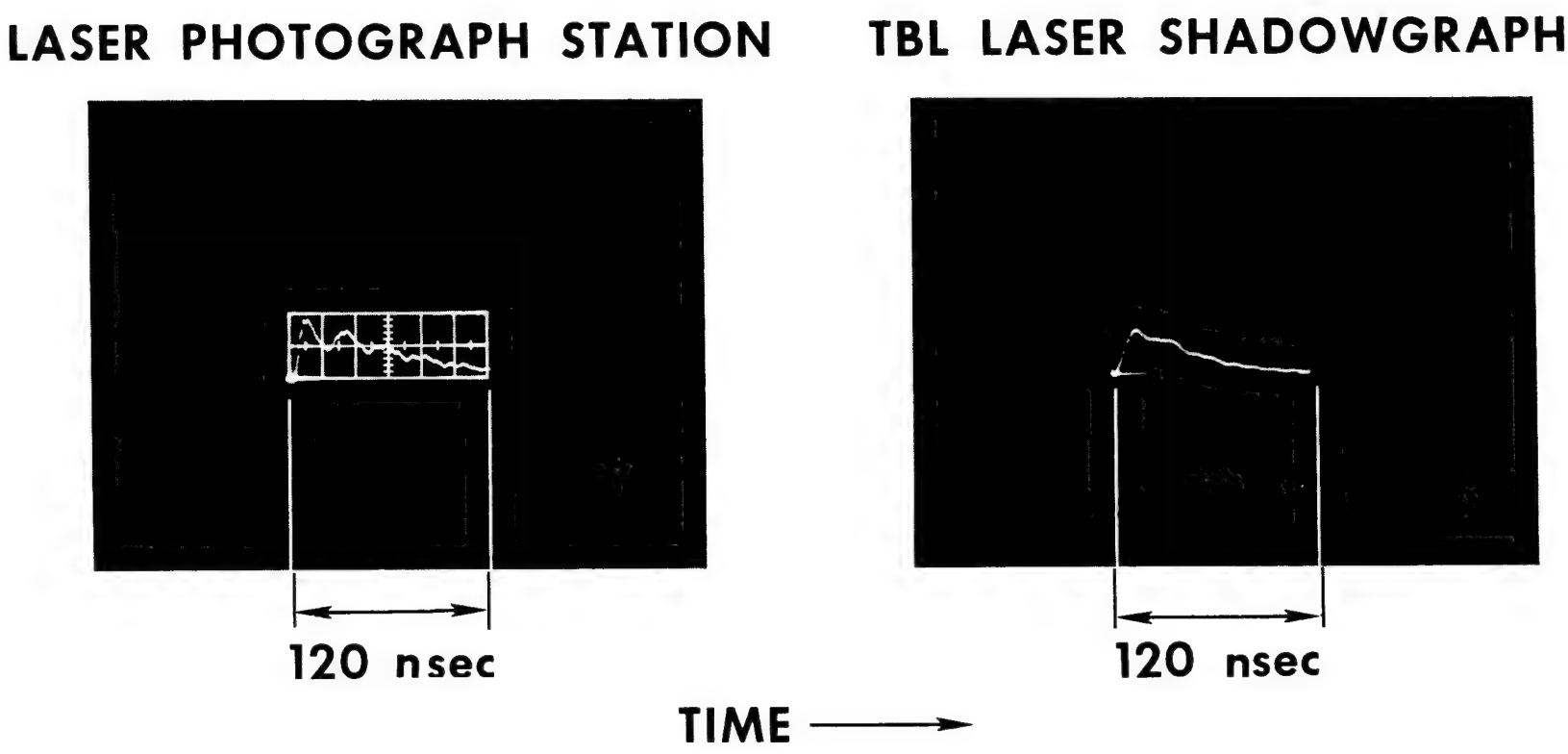

Figure 26 Time Duration of Laser Light Pulses

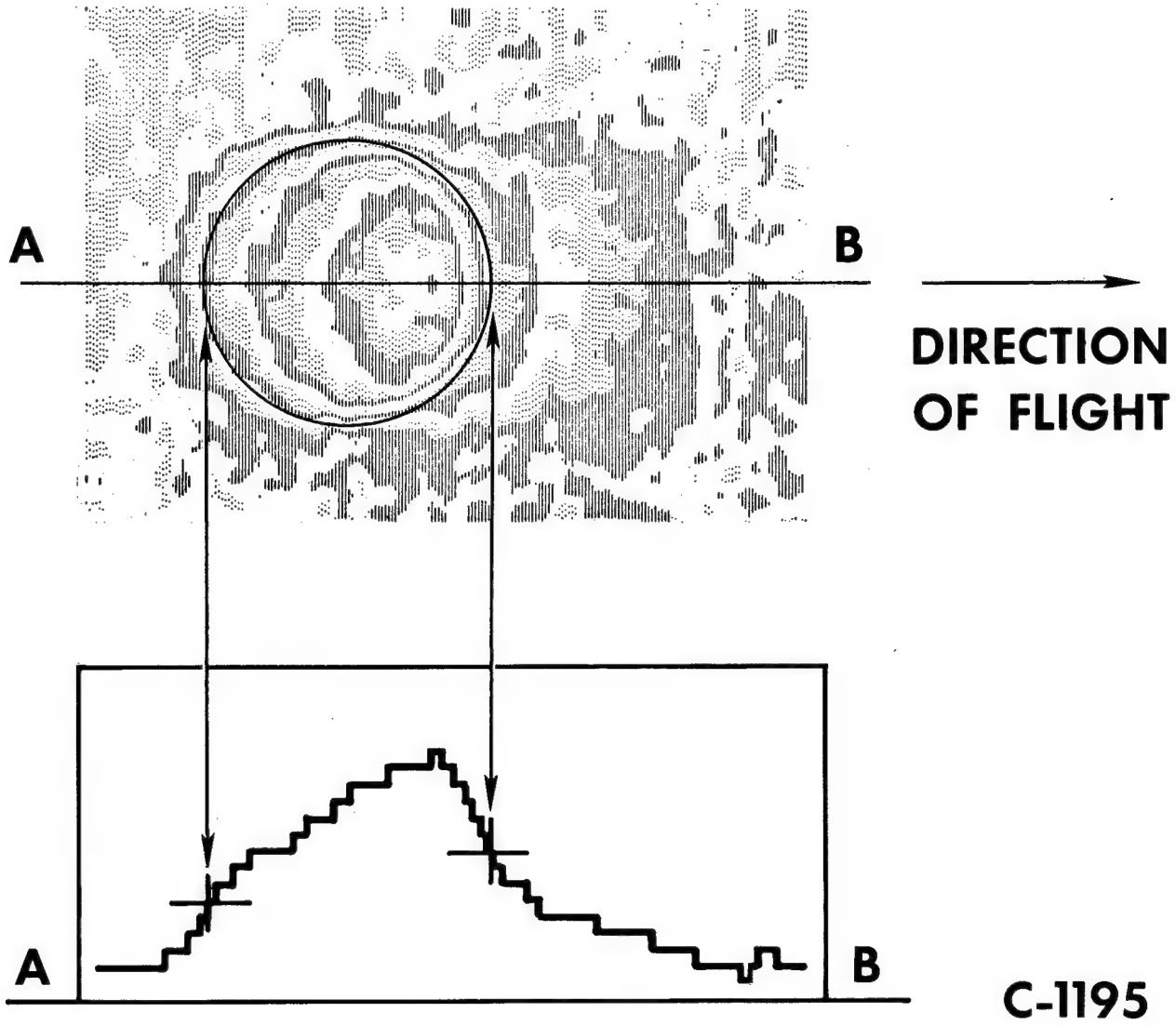

Figure 27 Principle Image, C-1195

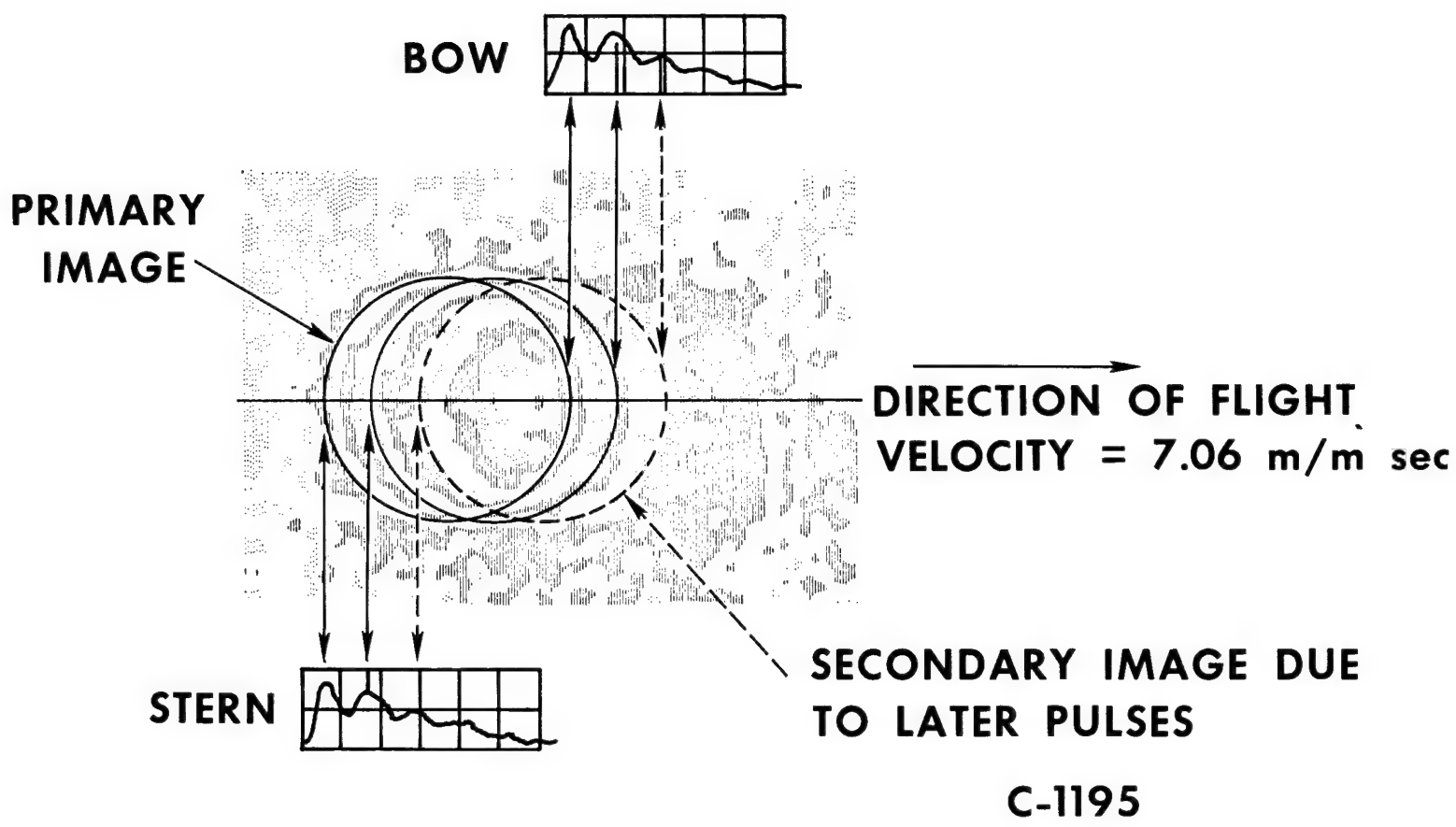

Figure 28 Time Correlation of Isodensity Record with Laser Output

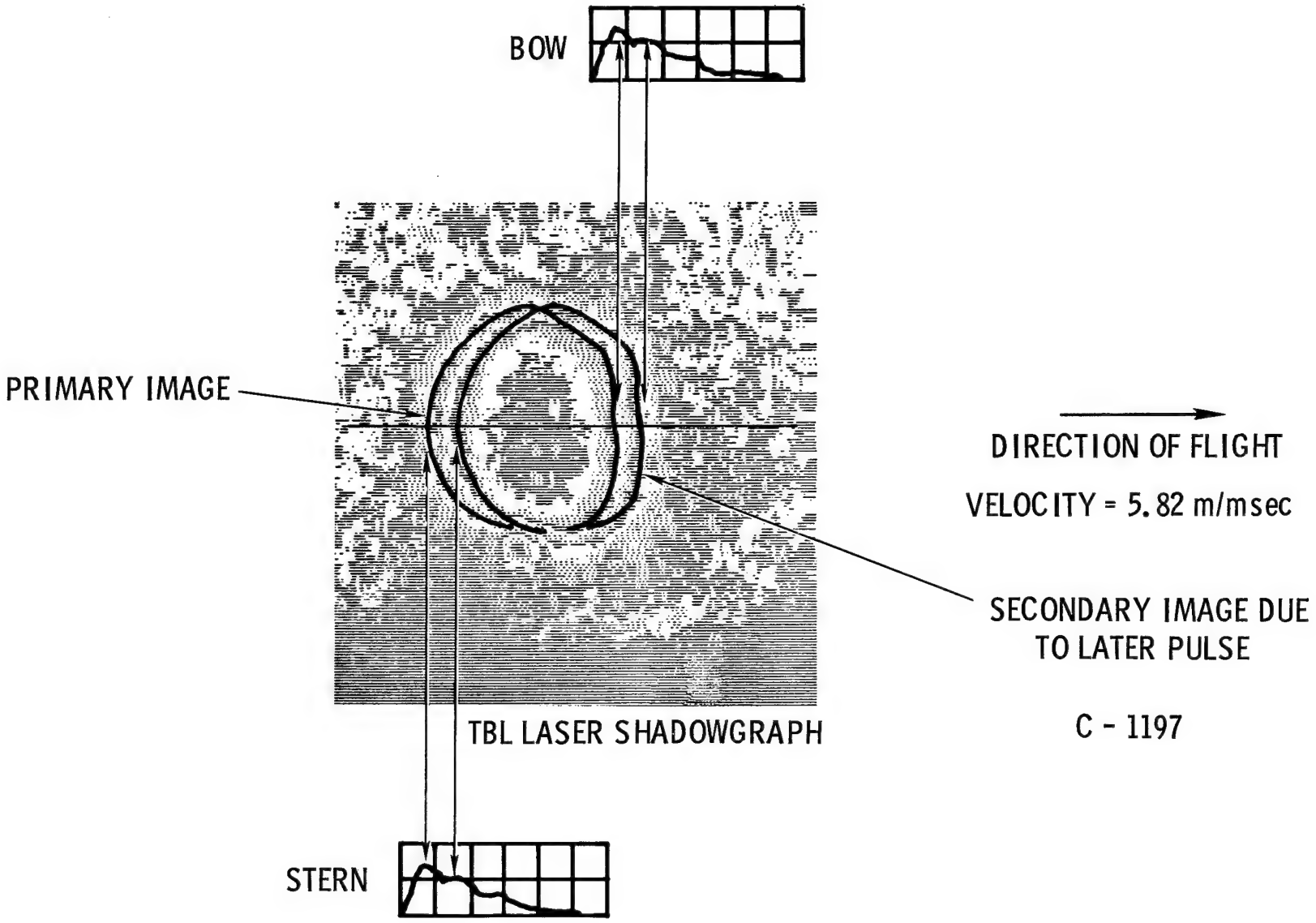

Figure 29 Time Correlation of Isodensity Record with TBL Laser Output

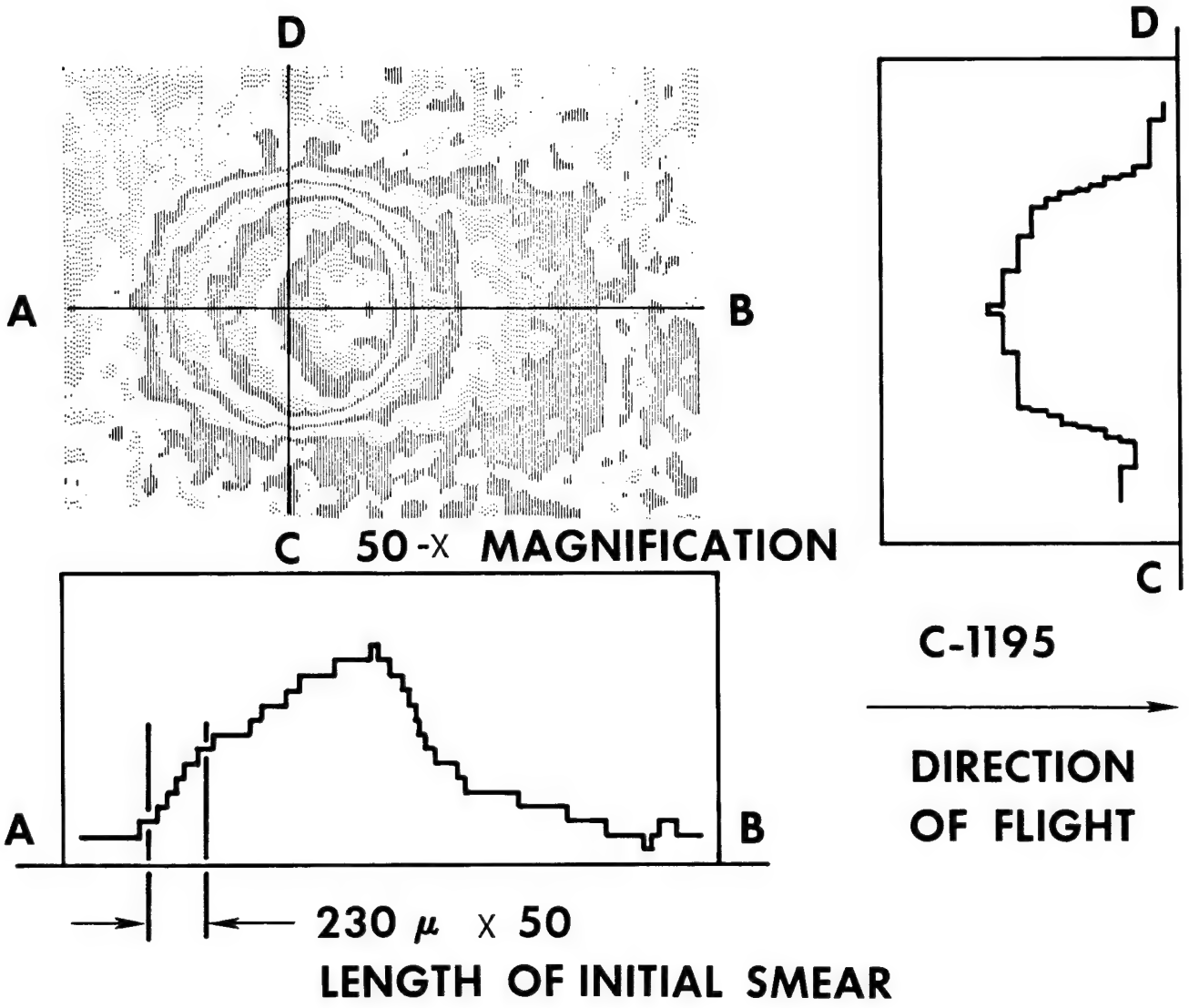

Figure 30 Isodensity Record for C-1195 Showing Smear for Laser Photograph

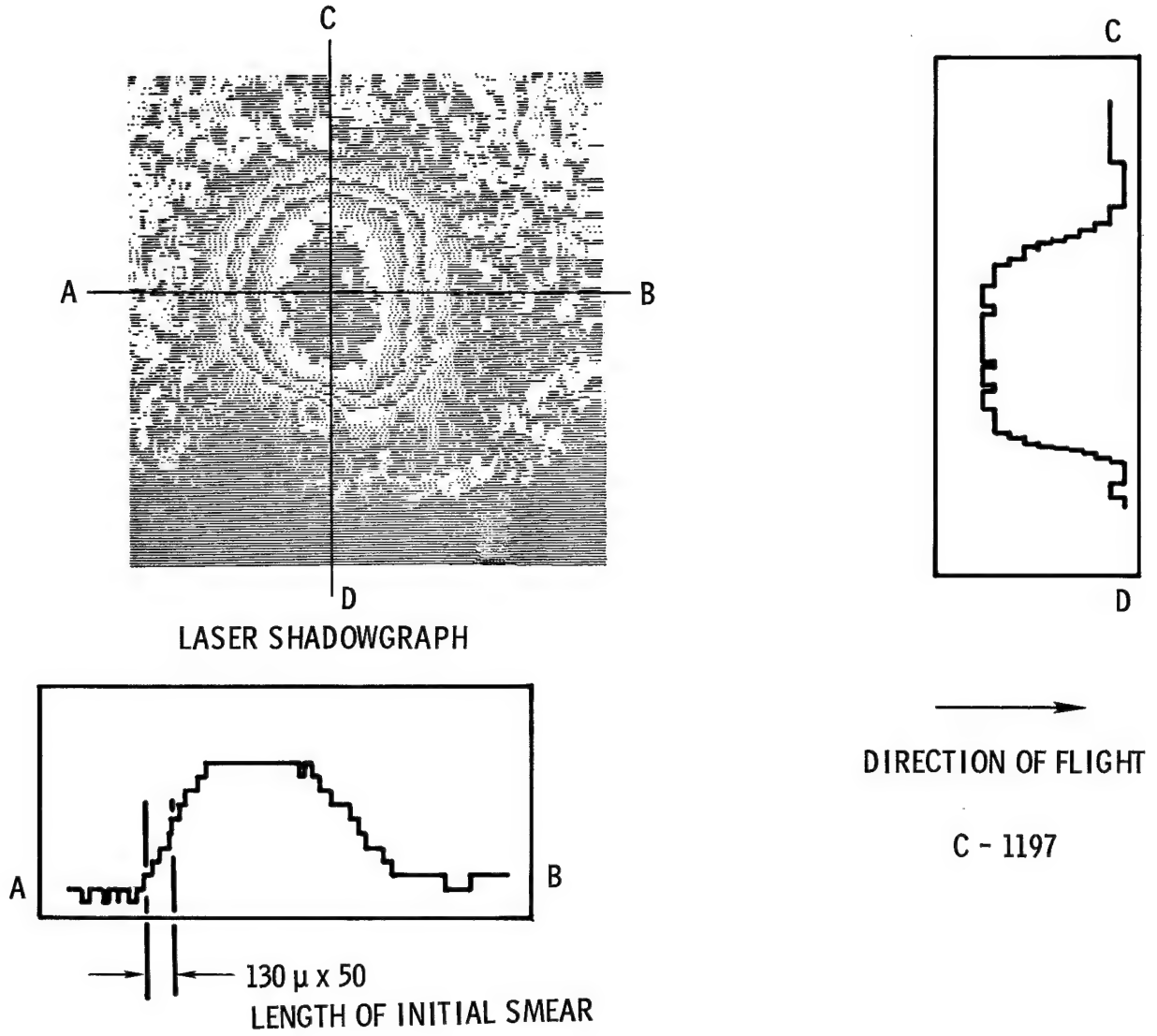

Figure 31 Isodensity Record for C-1197 Showing Smear for TBL Laser Shadowgraph Station

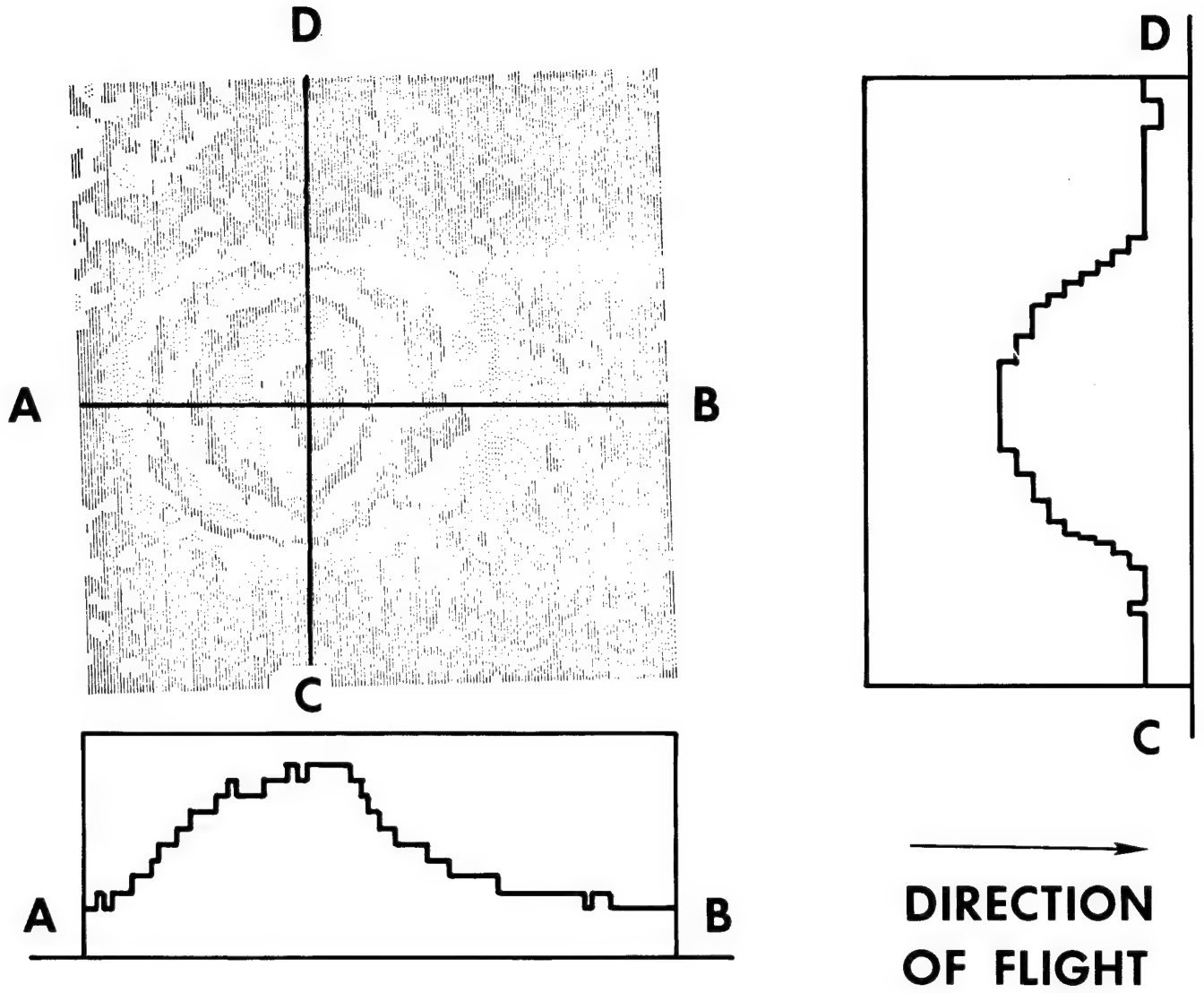

Figure 32 Isodensity Record for C-1196

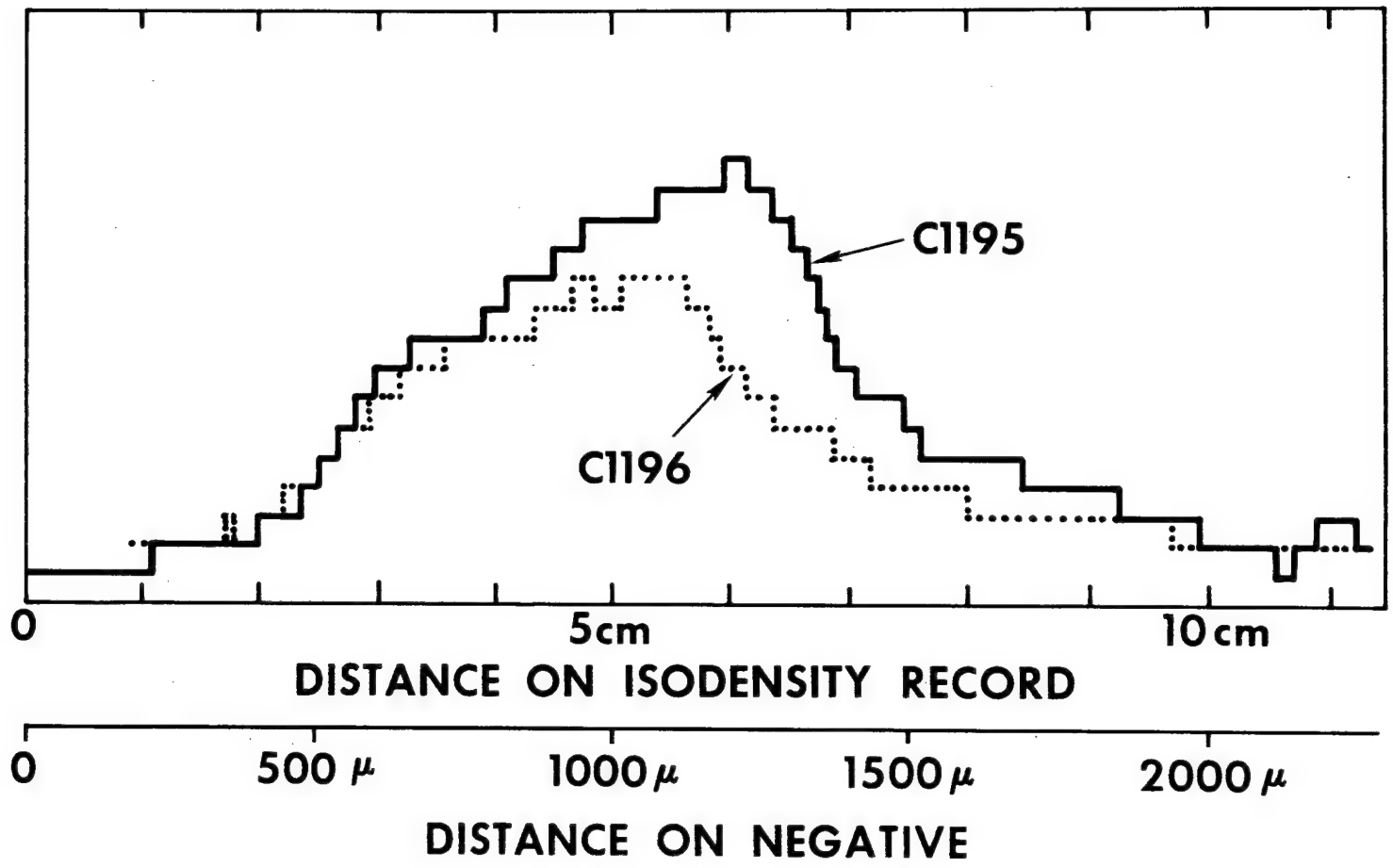

Figure 33 Comparison of Density Profile of Rounds C-1195 and C-1196

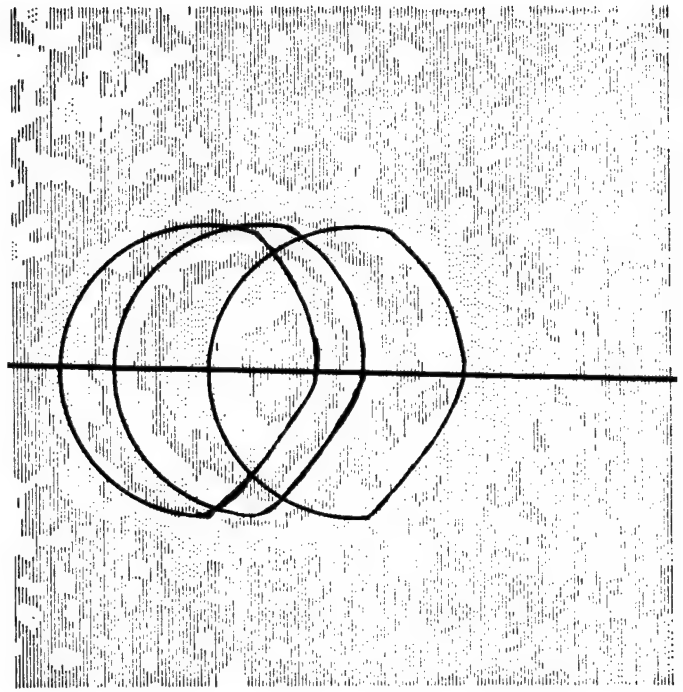

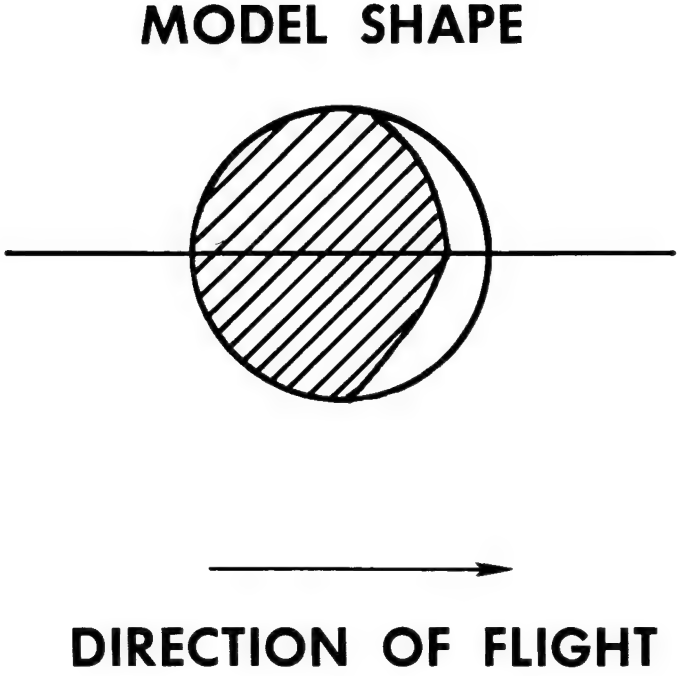

Figure 34 Particle Shape Determination for C-1196

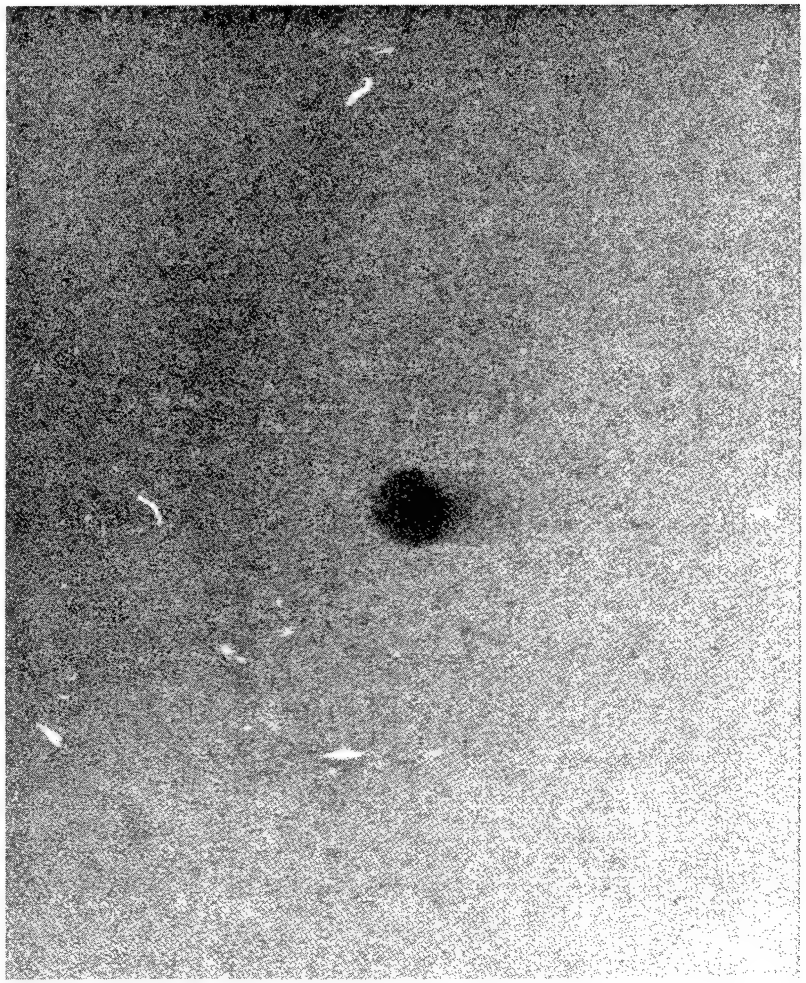

Figure 35 Enlargement of Laser Shadowgraph, C-1209

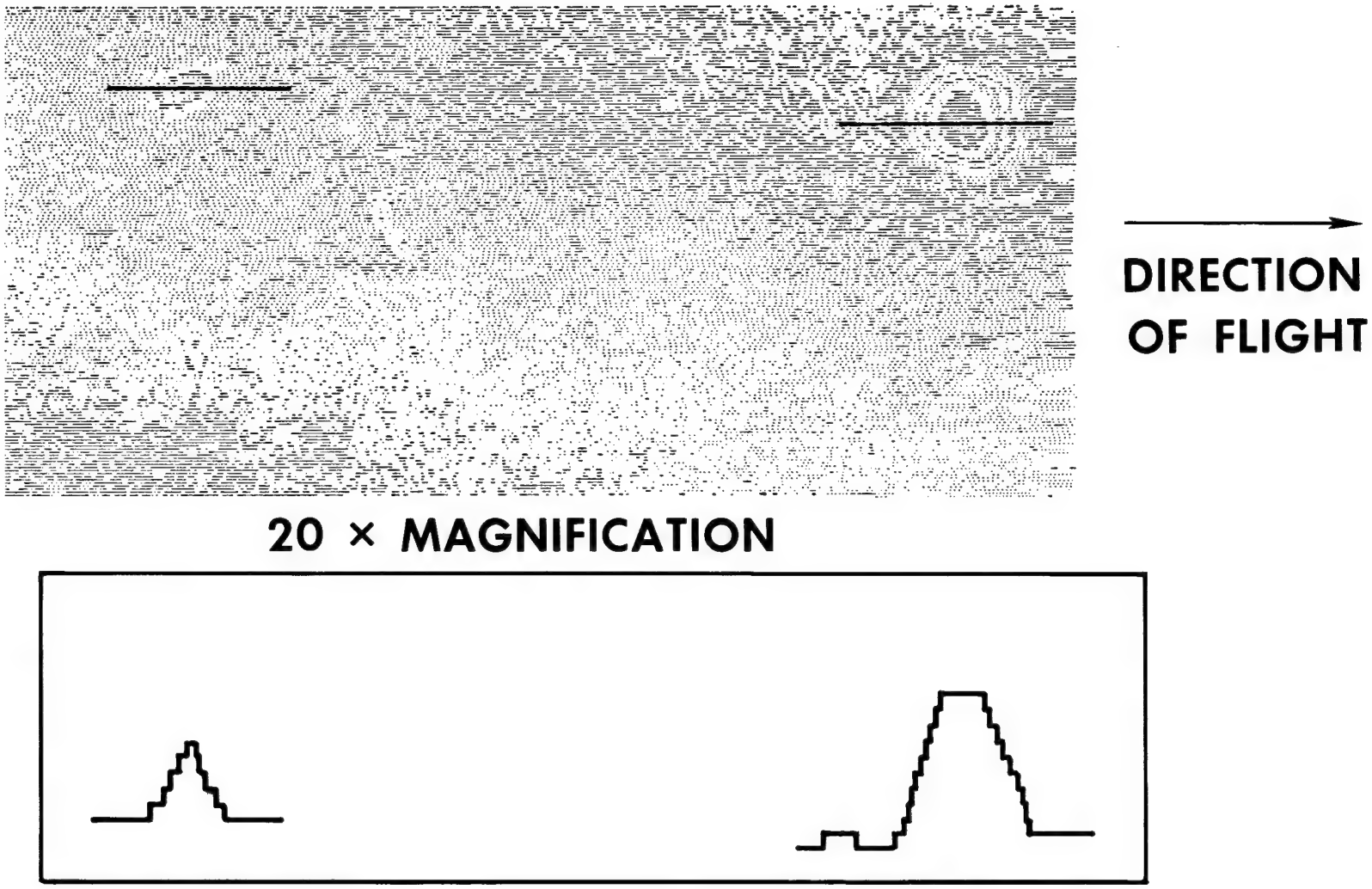

Figure 36 Isodensity Record Showing Two Particles, Round C-1197

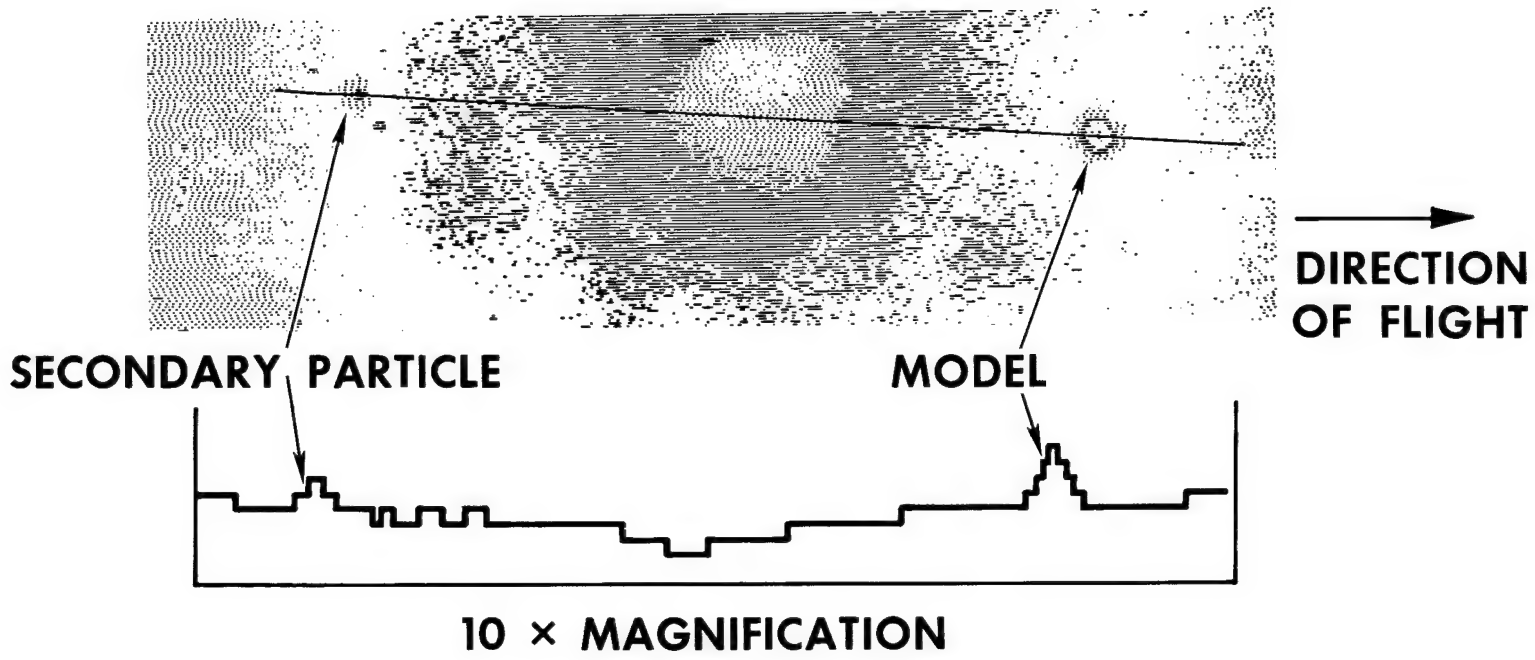

Figure 37 Isodensity Record Showing Two Particles, Round C-1202

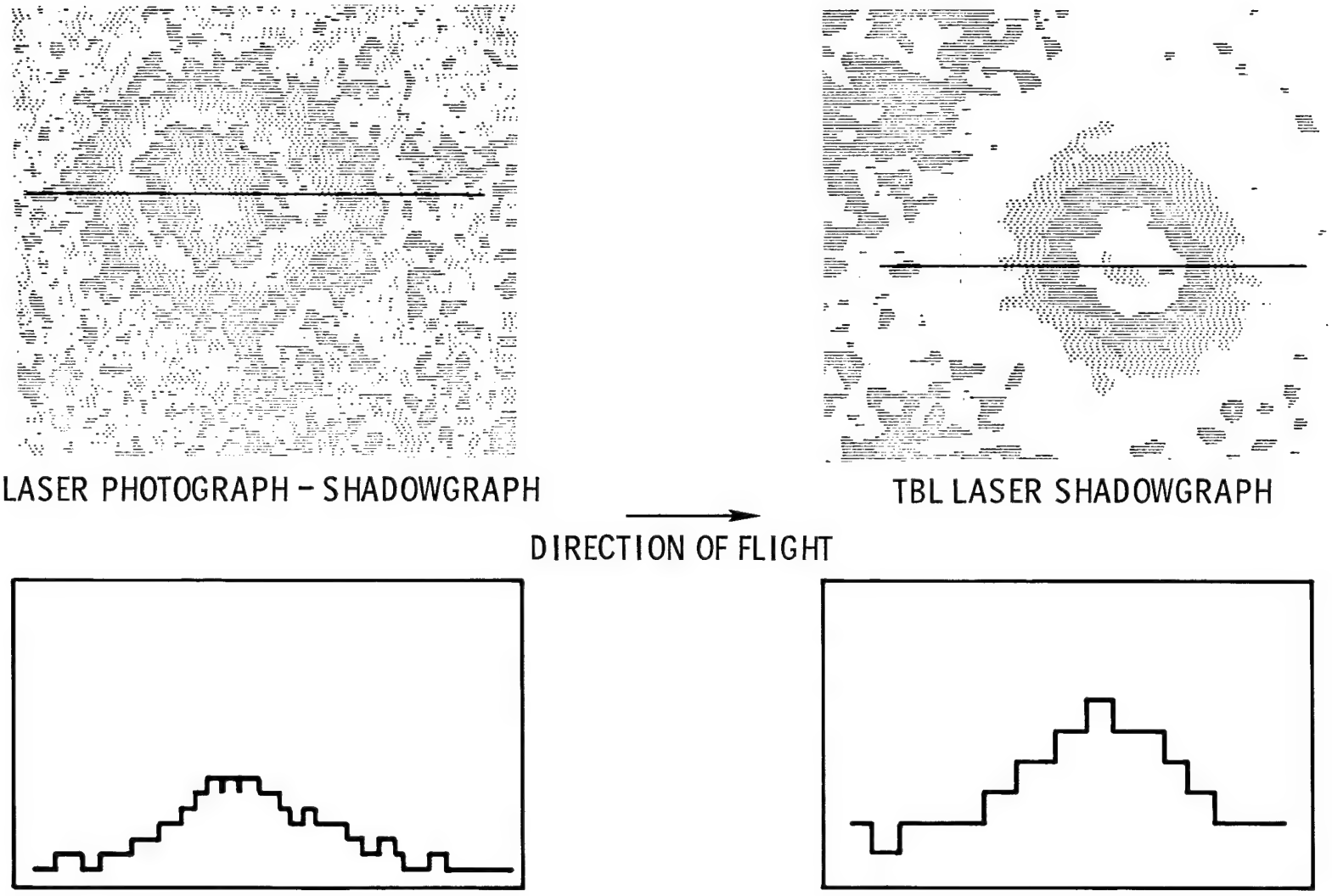

Figure 38 Shape Determination, Round C-1202

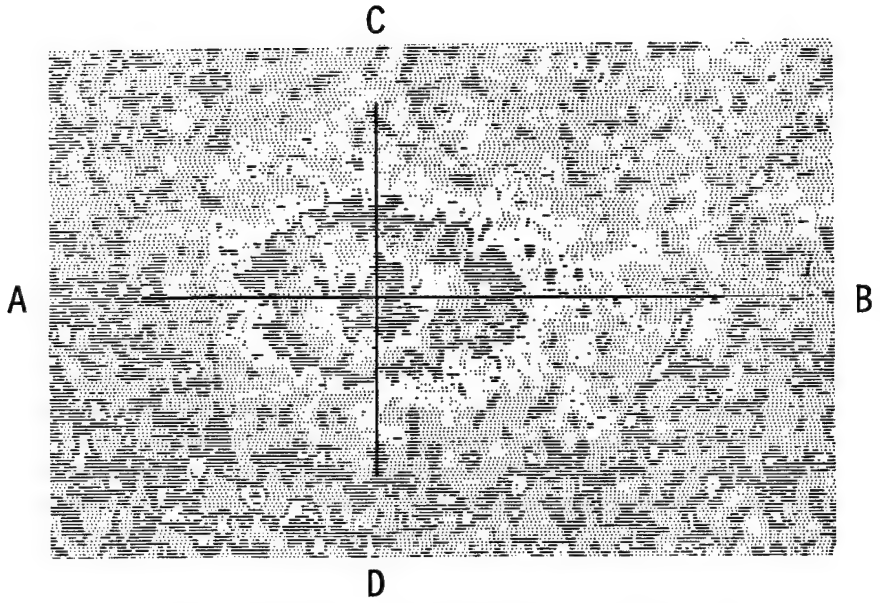

LASER PHOTOGRAPH - SHADOWGRAPH

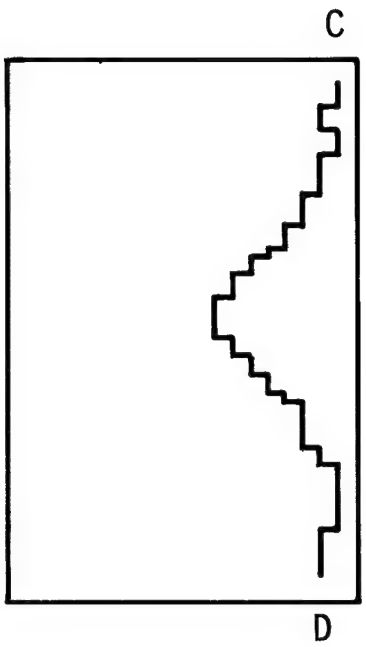

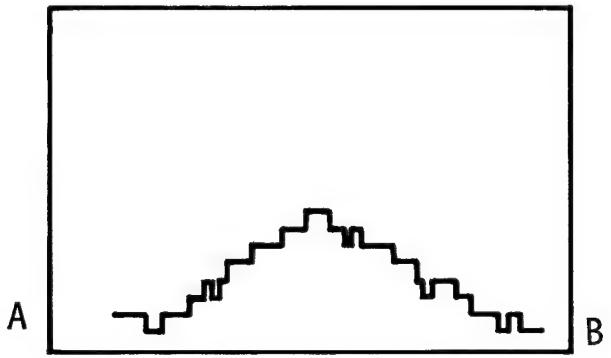

DIRECTION OF FLIGHT

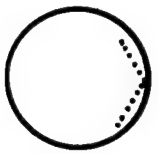

MODEL SHAPE

Figure 39 Shape Determination, Round C-1210

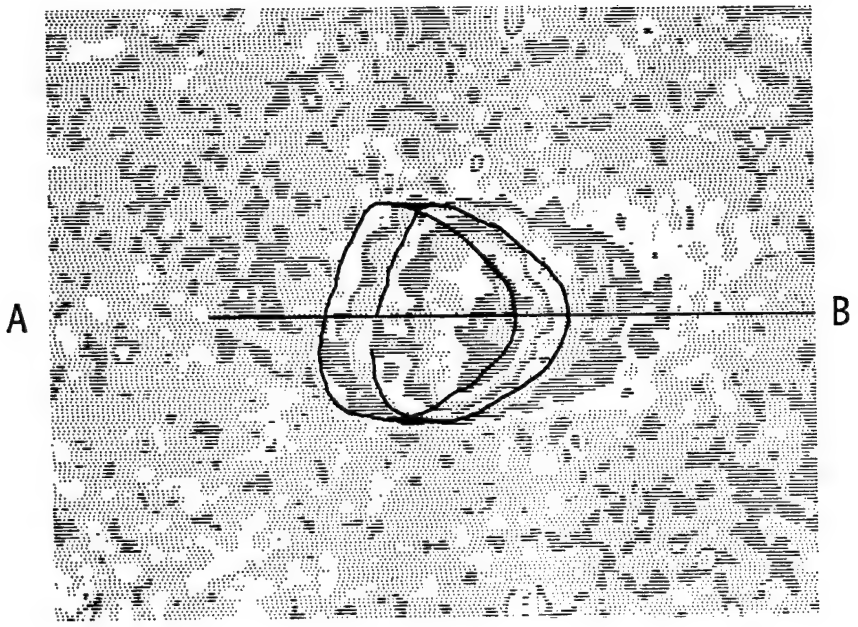

LASER PHOTOGRAPH STATION - SHADOWGRAPH

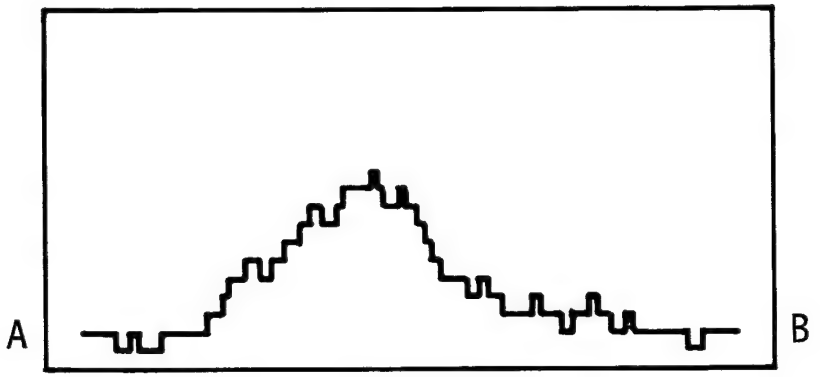

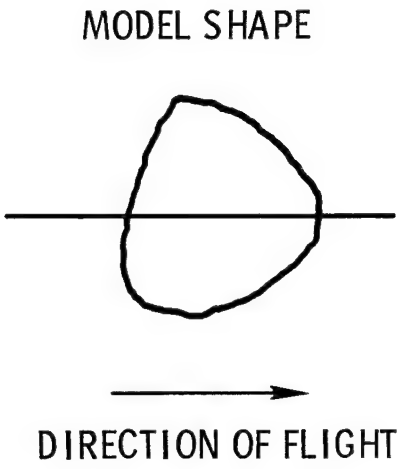

Figure 40 Shape Determination, Round C-1211

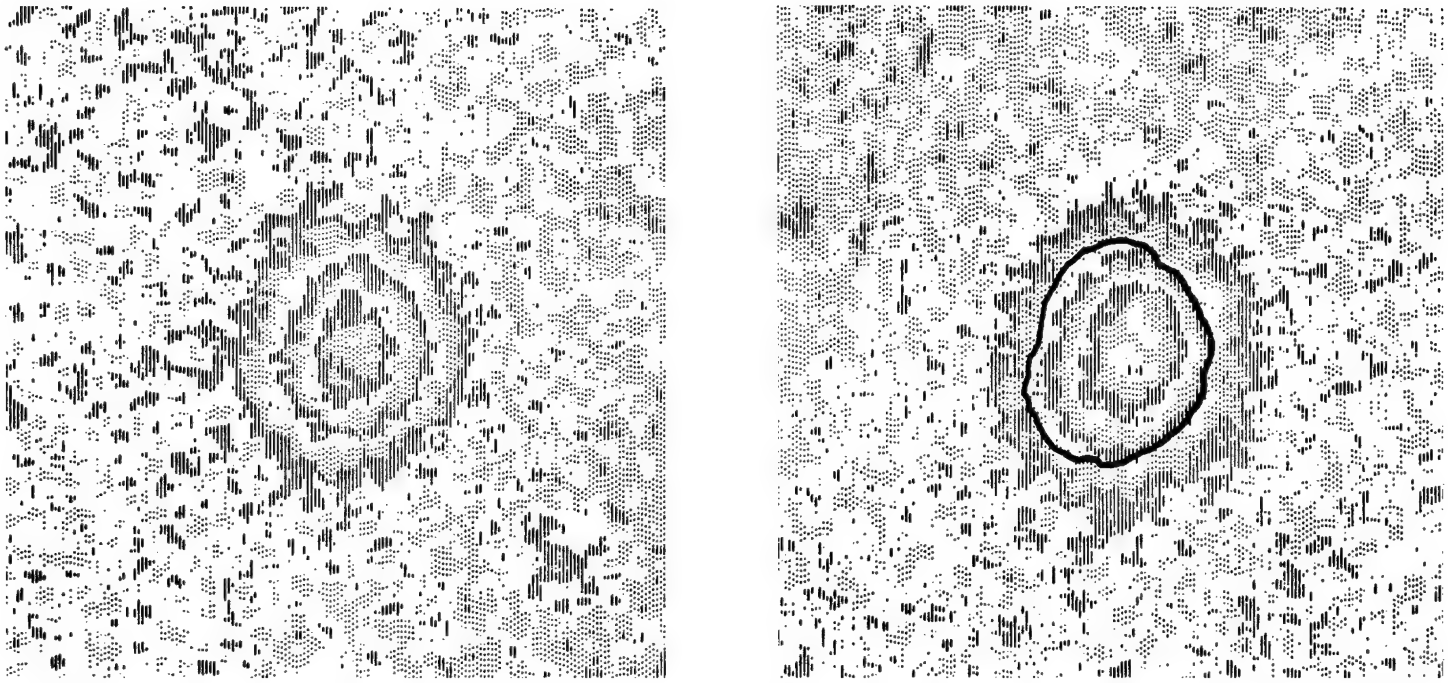

Figure 41 Particle Breakup, Round C-1211

DISTRIBUTION FOR SC-CR-66-2128
FEASIBILITY STUDY ON SMALL PARTICLE ABLATION
USING A FREE-FLIGHT RANGE

DISTRIBUTION:

U. S. Atomic Energy Commission
Director, Space Nuclear Systems
Space Electric Power Office
Washington, D. C. 20545
Attn: G. P. Dix, Chief, Safety Branch

U. S. Atomic Energy Commission
Director, Space Nuclear Systems
Space Electric Power Office
Washington, D. C. 20545
Attn: R. S. Decker, Jr., Chief, Safety Branch

U. S. Atomic Energy Commission
Director, Space Nuclear Systems
Space Electric Power Office
Washington, D. C. 20545
Attn: W. A. Yingling

U. S. Atomic Energy Commission
Director, Space Nuclear Systems
Space Electric Power Office
Washington, D. C. 20545
Attn: R. T. Carpenter
Chief, Isotope Power Systems Branch

U. S. Atomic Energy Commission
Director, Space Nuclear Systems
Space Electric Power Office
Washington, D. C. 20545
Attn: H. Specter
Reactor Power Systems Branch

U. S. Atomic Energy Commission
Space Nuclear Propulsion Office
Albuquerque Extension
Albuquerque Operations Office
P. O. Box 5400
Albuquerque, New Mexico
Attn: H. P. Smith

U. S. Atomic Energy Commission
Division of Isotope Development
Washington, D. C. 20545
Attn: W. K. Kern

U. S. Atomic Energy Commission
Division of Safety Standards (Beth 010)
Washington, D. C. 20545
Attn: J. J. Dinunno
Assistant Director, Reactors

U. S. Atomic Energy Commission
Division of Biology and Medicine
Washington, D. C. 20545
Attn: J. Z. Holland, Chief
Fallout Studies Branch

U. S. Atomic Energy Commission
Division of Biology and Medicine
Washington, D. C. 20545
Attn: H. D. Bruner, Asst. Director
Medical and Health Research

U. S. Atomic Energy Commission (3)
Division of Technical Information
Headquarters Library G-017
Washington, D. C. 20545

U. S. Atomic Energy Commission
Albuquerque Operations Office
P. O. Box 5400
Albuquerque, New Mexico 87115
Attn: S. A. Upson, Director
Research and Classification Division

U. S. Atomic Energy Commission
Albuquerque Operations Office
P. O. Box 5400
Albuquerque, New Mexico
Attn: V. C. Vespe, Director
Operational Safety Division

U. S. Atomic Energy Commission
Canoga Park Area Office
P. O. Box 591
Canoga Park, California
Attn: C. R. Malmstrom

U. S. Atomic Energy Commission
Chicago Operations Office
9800 South Cass Avenue
Argonne, Illinois 60439
Attn: Chief, Office Services Branch

U. S. Atomic Energy Commission
Oak Ridge Operations Office
Mail and Document Accountability Section
P. O. Box E
Oak Ridge, Tennessee 37831
Attn: Director, Research and Development Division

Headquarters
Air Force Systems Command (SCIZN)
Washington, D. C. 20331
Attn: Nuclear Safety Branch

Air Force Weapons Laboratory
Kirtland Air Force Base, New Mexico
Attn: Lt. Col. H. L. Harris (WLAS)

Air University Library
Maxwell Air Force Base, Alabama
Attn: Elizabeth C. Pittman

Atomics International (2)
P. O. Box 309
Canoga Park, California 91304
Attn: R. L. Detterman

Battelle Memorial Institute
505 King Avenue
Columbus, Ohio 43201
Attn: J. E. Davis, Projects Administrator

DISTRIBUTION (cont)

Battelle Memorial Institute
Pacific Northwest Laboratory
P. O. Box 999
Richland, Washington 99352
Attn: E. A. Coppinger

Battelle Memorial Institute
Pacific Northwest Laboratory
P. O. Box 999
Richland, Washington 99352
Attn: Dr. Roy Thompson

Battelle Memorial Institute
Pacific Northwest Laboratory,
P. O. Box 999
Richland, Washington 99352
Attn: M. T. Walling

The Boeing Company
Aerospace Group
P. O. Box 3707
Seattle, Washington 98124
Attn: T. L. Smith, Mail Stop 23-82

Brookhaven National Laboratory
Technical Information Division
Upton, Long Island, New York 11973
Attn: Research Library

Director, Defense Atomic Support Agency
P. O. Box 2610
Washington, D. C. 20301
Attn: Document Library Branch

Douglas Aircraft Company, Inc.
Missile and Space Systems Division
3000 Ocean Park Boulevard
Santa Monica, California
Attn: Sig Gronich
Advanced Space Technology

E. I. Du Pont De Nemours and Company
Savannah River Laboratory
Aiken, South Carolina 29802
Attn: W. B. Scott, Document Division

General Atomic Division
General Dynamics Corporation
P. O. Box 608
San Diego, California 92112
Attn: Library

General Electric Company
Nuclear Materials and Propulsion Operation
P. O. Box 15132
Cincinnati, Ohio 45215
Attn: J. W. Stephenson
For: W. Briskin

General Electric Company
Valley Forge Space Technology Center
P. O. Box 8555
Philadelphia, Pennsylvania 19101
Attn: S. M. Scala, Room M9539
Space Sciences Laboratory

General Electric Company
Valley Forge Space Technology Center
P. O. Box 8555
Philadelphia, Pennsylvania 19101
Attn: Carl Gamertsfelder
Advanced Requirements Planning Dept.

General Electric Company
570 Lexington Avenue
New York, New York 10022
Attn: Richard W. Porter, Consultant
Aerospace Science and Technology

Hittman Associates, Inc.
P. O. Box 2685
4715 East Wabash Avenue
Baltimore, Maryland, 21215

Institute for Defense Analyses
400 Army Navy Drive
Arlington, Virginia 22200
Attn: Richard Briceland

Lockheed Missiles and Space Company
P. O. Box 504
Sunnyvale, California
Attn: H. H. Greenfield, Manager
Nuclear Power Development

Lockheed Missiles and Space Company
P. O. Box 504
Sunnyvale, California
Attn: R. F. Hausman (Dept. 30-63)
Cryogenic and Nuclear Stage Programs

Lockheed Missiles and Space Company
P. O. Box 504
Sunnyvale, California
Attn: Harold F. Plank

Los Alamos Scientific Laboratory (3)
P. O. Box 1663
Los Alamos, New Mexico 87544
Attn: Dr. L. D. P. King
F. W. Schonfeld, CMF-5
C. F. Metz, CMB-1

Deputy I. G. for Insp. and Safety, USAF
Kirtland Air Force Base, New Mexico 87117
Attn: Col. D. C. Jameson (AFINSR)

DISTRIBUTION (cont)

Nuclear Materials and Equipment Co.
Apollo, Pennsylvania 15613

Douglas Aircraft Company, Inc.
Missile and Space System Division
3000 Ocean Park Boulevard
Santa Monica, California
Attn: John Watcher
Advanced Space Technology

Los Alamos Scientific Laboratory
P. O. Box 1663
Los Alamos, New Mexico 87544
Attn: Dr. Wright Langham

Lovelace Foundation for Medical Education
and Research
5200 Gibson Blvd., SE
Albuquerque, New Mexico
Attn: Dr. C. S. White, President-Director

Martin Company
Nuclear Programs
Middle River, Maryland 21203
Attn: D. G. Harvey, Mail No. 801

Minnesota Mining and Manufacturing Co.
2501 Hudson Road, Maplewood
St. Paul, Minnesota 55119
Attn: J. P. Ryan, TCAAP 675
Nuclear Products Department

Monsanto Research Corporation
Mound Laboratory
P. O. Box 32
Miamisburg, Ohio 45342
Attn: G. R. Grove

Administrator
National Aeronautics and Space Administration
Washington, D. C. 20545
Attn: T. B. Kerr (RNS)

National Aeronautics and Space Administration
Ames Research Center
Moffet Field, California
Attn: Glenn Goodwin (1)
For: Dean Chapman (1)

National Aeronautics and Space Administration
Goddard Space Flight Center
Glenn Dale Road
Greenbelt, Maryland 20771
Attn: A. W. Fihelly, Nimbus Project

National Aeronautics and Space Administration
Lewis Research Center
21000 Brookpark Road
Cleveland, Ohio 44135
Attn: Library

National Aeronautics and Space Administration
Manned Spacecraft Center
Houston, Texas 77058
Attn: Technical Information Dissemination
Branch (Code BM6)

National Aeronautics and Space Administration (2)
Scientific and Technical Information Facility
P. O. Box 33
College Park, Maryland 20740
Attn: Acquisitions Branch (S-AK/DL)

NUS Corporation
Environmental Safeguards Division
Suite 1100
1730 M Street, N. W.
Washington, D. C. 20036
Attn: M. S. Goldman, Vice President

Phillips Petroleum Company
NRTS Technical Library
P. O. Box 2067
Idaho Falls, Idaho 83401

Radio Corporation of America
Astro Electronics Division
P. O. Box 800
Princeton, New Jersey 08540
Attn: S. H. Winkler
Ldr. Adv. Power

Director, USAF Project RAND
via Air Force Liaison Office
The Rand Corporation
1700 Main Street
Santa Monica, California 90406
Attn: Library

Space Nuclear Propulsion Office
Lewis Research Center
21000 Brookpark Road
Cleveland, Ohio 44135
Attn: L. Nichols

TRW Systems
P. O. Box 287
Redondo Beach, California 90278
Attn: Dr. Donald Jortner

U. S. Naval Radiological Defense Laboratory
Commanding Officer and Director
San Francisco, California 94135
Attn: P. E. Zigman

Union Carbide Corporation (2)
Nuclear Division
P. O. Box X
Oak Ridge, Tennessee 37831
Attn: B. R. Fish, Health Physics Division

DISTRIBUTION (cont):

GM Defense Research Laboratories
General Motors Corporation
Santa Barbara, California
Attn: D. J. Collins (2)

National Aeronautics and Space Administration
Ames Research Center
Moffet Field, California
Attn: W. A. Page

National Aeronautics and Space Administration
Ames Research Center
Moffet Field, California
Attn: John Given

University of California
Lawrence Radiation Laboratory
P.O. Box 808
Livermore, California 94551
Attn: Technical Information Division

Westinghouse Electric Company
Astronuclear Laboratory
P.O. Box 10864
Pittsburgh 30, Pennsylvania
Attn: Joanne M. Bridges, Supervisor
Flight Safety Analysis Group

Division of Technical Information Extention (70)
U.S. Atomic Energy Commission
P.O. Box 62
Oak Ridge, Tennessee 37831

Union Carbide Research Institute
P.O. Box 278
Tarrytown, New York
Attn: Joseph Agresta, Space Sciences Group

Input Section
Clearinghouse (75)
5285 Port Royal Road
Springfield, Virginia 22151

University of California
Lawrence Radiation Laboratory
P.O. Box 808
Livermore, California 94551
Attn: Dr. James Hadley, Chief, R. Division

J. R. Banister, 5120
J. D. Shreve, 5234
L. S. Nelson, 5234
D. B. Shuster, 5600
W. T. Moffat, 7220
H. E. Viney, 7250
L. E. Lamkin, 7300
G. A. Fowler, 9000
J. H. Scott, 9200
V. E. Blake, 9310
H. E. Hansen, 9311
H. L. Hodges, 9311
S. L. Jeffers, 9312
S. McAlees, Jr., 9314
R. J. Everett, 9315
J. D. Appel, 9319
J. D. Appel, 9319, ANSIC (2)
R. C. Maydew, 9320
H. R. Vaughn, 9321
K. J. Touryan, 9326
W. A. Klikoff, 9326
A. J. Clark, 9330
J. W. McKiernan, 9331
L. C. Baldwin, 3412
E. A. Paxton, 8232
B. R. Allen, 3421
W. K. Cox, 3428-1
R. S. Gillespie, 3413
Attn: J. G. Wallace, 3413
C. H. Sproul, 3428-2 (5)